

## Silver Baits for The “Miraculous Draught” of Amphiphilic Lanthanide Helicates

Emmanuel Terazzi,<sup>\*,[a]</sup> Laure Guénée,<sup>[a]</sup> Johan Varin,<sup>[a]</sup> Bernard Bocquet,<sup>[a]</sup>  
Jean-François Lemonnier,<sup>[a]</sup> Daniel Emery,<sup>[b]</sup> Jiri Mareda,<sup>\*,[b]</sup> and Claude Piguet<sup>\*,[a]</sup>

**Abstract:** The axial connection of flexible thioalkyl chains of variable length ( $n=1-12$ ) within the segmental bis-tridentate 2-benzimidazole-8-hydroxyquinoline ligands  $[\mathbf{L12}^{Cn}-2\text{H}]^{2-}$  provides amphiphilic receptors designed for the synthesis of neutral dinuclear lanthanide helicates. However, the stoichiometric mixing of metals and ligands in basic media only yields intricate mixtures of poorly soluble aggregates. The addition of  $\text{Ag}^{\text{I}}$  in solution restores classical helicate architectures for  $n=3$ , with the quantitative formation of the discrete  $D_3$ -symmetrical  $[\text{Ln}_2\text{Ag}_2(\mathbf{L12}^{C3}-2\text{H})_3]^{2+}$  complexes at millimolar concentration ( $\text{Ln}=\text{La}, \text{Eu}, \text{Lu}$ ).

The X-ray crystal structure supports the formation of  $[\text{La}_2\text{Ag}_2(\mathbf{L12}^{C3}-2\text{H})_3][\text{OTf}]_2$ , which exists in the solid state as infinite linear polymers bridged by S-Ag-S bonds. In contrast, molecular dynamics (MD) simulations in the gas phase and in solution confirm the experimental diffusion measurements, which imply the formation of discrete molecular entities in these media, in which the sulfur atoms of each lipophilic

ligand are rapidly exchanged within the  $\text{Ag}^{\text{I}}$  coordination sphere. Turned as a predictive tool, MD suggests that this  $\text{Ag}^{\text{I}}$  templating effect is efficient only for  $n=1-3$ , while for  $n>3$  very loose interactions occur between  $\text{Ag}^{\text{I}}$  and the thioalkyl residues. The subsequent experimental demonstration that only 25% of the total ligand speciation contributes to the formation of  $[\text{Ln}_2\text{Ag}_2(\mathbf{L12}^{C12}-2\text{H})_3]^{2+}$  in solution puts the bases for a rational approach for the design of amphiphilic helical complexes with predetermined molecular interfaces.

**Keywords:** helical structures • heterometallic complexes • lanthanides • molecular dynamics • polynuclear complexes • silver

### Introduction

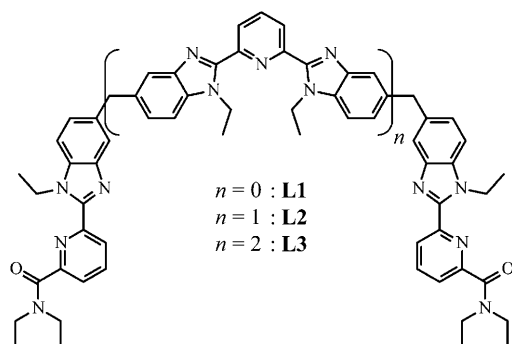
Metallohelicates, that is, polynuclear complexes made up of several metal ions packed along a helical axis, about which one, two, three, or four multidentate segmental ligands are wrapped, represent the archetype of discrete chemical enti-

ties, in which metallic cations are aligned along a single direction of the space.<sup>[1]</sup> Beyond some remarkable geometrical aspects (helical chirality, precursors for nontrivial molecular catenanes and knots, etc.), the helical twist of the strands also induces unprecedented magnetic and luminescent properties when adequate open-shell d-block or f-block metals are considered.<sup>[2-6]</sup> In molecular magnetism, the ligand helicity is responsible for the existence of non-equivalent metal-centered paramagnetic  $g$  tensors, which is a prerequisite for building scalable quantum bits (qubits) for quantum information processing systems.<sup>[2-4]</sup> In photophysics, the minute modulation of the luminescent properties of trivalent lanthanides ( $\text{Ln}^{\text{III}}$ ) in polynuclear helicates have been intensively exploited for the design of bioprobes with improved sensitivities,<sup>[5]</sup> and for the development of nanometric directional molecular light-converting devices.<sup>[6]</sup> In this context, the segmental oligo-tridentate ligands **L1-L3** based on pyridine-benzimidazole patterns were early considered as attractive candidates because of 1) their easy synthetic access, 2) their helically twisted diphenylmethane spacers, and 3) the energies of their donor excited triplet states, which are suitable

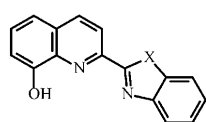
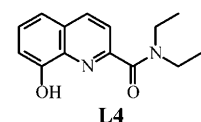
[a] Dr. E. Terazzi, Dr. L. Guénée, J. Varin, B. Bocquet, Dr. J.-F. Lemonnier, Prof. Dr. C. Piguet  
Department of Inorganic, Analytical and Applied Chemistry  
University of Geneva, 30 quai E. Ansermet  
1211 Geneva 4 (Switzerland)  
Fax: (+41)22-379-6830  
E-mail: Claude.Piguet@unige.ch  
Emmanuel.Terazzi@unige.ch

[b] D. Emery, Dr. J. Mareda  
Department of Organic Chemistry  
University of Geneva, 30 quai E. Ansermet  
1211 Geneva 4 (Switzerland)  
Fax: (+41)22-379-3215  
E-mail: Jiri.Mareda@unige.ch

Supporting information for this article is available on the WWW under <http://dx.doi.org/10.1002/chem.201002771>.



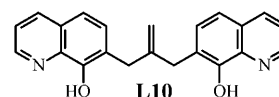
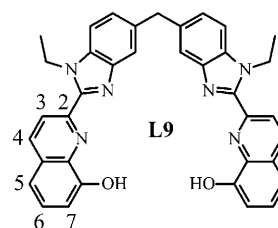
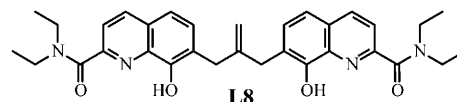
for the UV sensitization of visible  $\text{Eu}^{\text{III}}$  and  $\text{Tb}^{\text{III}}$  emitters in the triple-stranded helicates  $[\text{Ln}_2(\mathbf{L1})_3]^{6+}$ ,  $[\text{Ln}_3(\mathbf{L2})_3]^{9+}$  and  $[\text{Ln}_4(\mathbf{L3})_3]^{12+}$ .<sup>[7]</sup> However, the modern craze for profitable technological and/or (bio)medical applications of self-assembled lanthanide complexes introduced two additional criteria, which are difficult to fit simultaneously.<sup>[8,9]</sup> Firstly, the manipulation of near-infrared radiation (NIR) should be preferred over UV irradiations because 1) efficient and cheap laser sources are available at these wavelengths (Nd-YAG or  $\text{CO}_2$  lasers) and 2) biological tissues poorly interact with the electromagnetic waves in this domain, which ensures non invasive and efficient penetration of the NIR radiations.<sup>[8]</sup> Luminescent probes possessing intrashell  $4f \rightarrow 4f$  transitions in the NIR range ( $\text{Ln} = \text{Pr}, \text{Nd}, \text{Er}, \text{Yb}$ ) are now privileged, together with the use of suitable polyaromatic ligands, which are able to efficiently harvest low-energy visible light, prior to sensitize metal-centered excited states.<sup>[9]</sup> Secondly, practical applications require semi-organized luminescent lanthanide materials (liquid crystals, Langmuir-Blodgett films) responsive to switchable external stimuli (temperature, pressure, concentration, and electric and magnetic fields). Their design relies on weak intermolecular interactions operating between amphiphilic complexes possessing well-defined molecular interfaces separating their antinomic parts (polar/nonpolar for lyotropic materials or polarizable/nonpolarizable for their thermotropic analogues).<sup>[10]</sup> Pioneer attempts to fit these novel criteria have lead Albrecht,<sup>[11]</sup> Bünzli<sup>[12]</sup> and co-workers to replace the original pyridine-benzimidazole patterns with fused negatively charged 8-hydroxyquinolate in the tridentate ligands  $[\mathbf{Lk-H}]^-$  ( $k = 4-7$ ). The resulting mononuclear triple-helical



X = N-R : **L5**  
X = O : **L6**  
X = S : **L7**

$[\text{Ln}(\mathbf{Lk-H})_3]$  complexes indeed displayed  $\approx 10000 \text{ cm}^{-1}$  red-shifted ligand-centered electronic absorptions ( $\lambda_{\text{abs}}^{\text{max}} = 320 \text{ nm}$  (UV) for  $[\text{Ln}_2(\mathbf{L1})_3]^{6+}$  and  $470 \text{ nm}$  (Vis) for  $[\text{Ln}(\mathbf{L4-H})_3]$ ) compatible with the efficient visible sensitization of NIR luminescence for  $\text{Ln} = \text{Nd}, \text{Er}, \text{Yb}$ . While the X-ray crystal structures of  $[\text{Ln}(\mathbf{Lk-H})_3]$  ( $k = 4-7$ ) systematically corresponded to either pure  $C_1$ -symmetri-

cal HHT (head-to-head-to-tail) or  $C_3$ -symmetrical HHH (head-to-head-to-head) isomers in the solid state,  $^1\text{H NMR}$  data collected in solution revealed the presence of the expected thermodynamic 1:3 ratio of HHH and HHT isomers. To avoid mixtures, two identical related tridentate binding units were connected to a  $C_2$ -symmetrical spacer in the segmental ligands  $\mathbf{L8}^{[13]}$  and  $\mathbf{L9}^{[12a]}$ , and only the expected  $D_3$ -



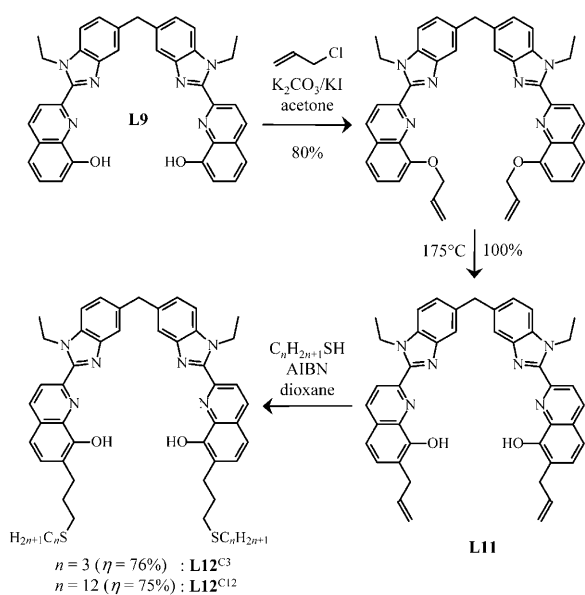
symmetrical triple-stranded helicates  $[\text{Ln}_2(\mathbf{Lk-2H})_3]$  ( $k = 8, 9$ , with a local HHH orientation of the three tridentate binding units connected to the same metal) could be evidenced in solution by  $^1\text{H NMR}$  spectroscopy. Interestingly, the crystal structure of  $\text{HHH-}[\text{KYb}_2(\mathbf{L8-2H})_3]\text{Cl}$  incorporated an additional  $\text{K}^+$  ion approximately located on the helical axis between the two nine-coordinate  $\text{Yb}^{\text{III}}$  cations ( $\text{Yb1} \cdots \text{K} = 3.91$ ,  $\text{K} \cdots \text{Yb2} = 3.95$ ,  $\text{Yb1} \cdots \text{Yb2} = 7.77 \text{ \AA}$ ).<sup>[13]</sup> Although the explicit templating effect of  $\text{K}^+$  in the self-assembly of  $[\text{KYb}_2(\mathbf{L8-2H})_3]^+$  remained obscure,<sup>[13]</sup> the report of the formation of mixtures of polymers for the closely related neutral dinuclear  $[\text{M}_2(\mathbf{L10-2H})_3]_{\infty}$  ( $\text{M} = \text{Al}, \text{Ga}, \text{Fe}, \text{Cr}$ ) complexes, which were transformed into soluble triple-stranded helicates  $[\text{M}'\text{M}_2(\mathbf{L10-2H})_3]^+$  ( $\text{M}' = \text{K}, \text{Rb}, \text{Cs}$ ) upon treatment with alkali-metal salts ( $\text{KCl}, \text{RbCl}, \text{CsCl}$ ), suggested that the monovalent ion  $[\text{M}']^+$  was crucial for the stabilization of the final discrete helical edifices.<sup>[14]</sup> In contrast, no additional templating cation could be found in the crystal structure of the triple-stranded  $[\text{Nd}_2(\mathbf{L9-2H})_3]$  helicate ( $\text{Nd1} \cdots \text{Nd2} = 9.02-9.05 \text{ \AA}$ ).<sup>[15]</sup> Altogether, the triple-stranded helicates  $[\text{Ln}_2(\mathbf{L9-2H})_3]$  offer an unprecedented opportunity for designing dinuclear NIR emitters, in which the grafting of flexible chains onto the 7-position of the hydroxyquinoline ring (**L9**) may provide the necessary molecular interface compatible with the design of amphiphilic complexes having potential technological applications (thermotropic liquid crystals or bioanalytical probes). Moreover, secondary interactions with some additional cations may contribute to modulate the stability and the properties of the final edifices without resorting to tedious synthetic modifications of the ligands.

In this contribution, we report on an appealing templating effect which controls the formation of amphiphilic supra-

molecular complexes containing a standard rigid dinuclear lanthanide triple-stranded helical core, to which several bulky lipophilic thioalkyl chains are axially grafted for extending the helical strands. The design of these novel systems was assisted by molecular dynamics (MD) simulations.

## Results and Discussion

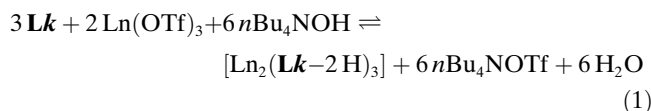
**Synthesis of ligands and of lanthanide complexes:** The target 7,7'-disubstituted bis-tridentate amphiphilic ligands **L12<sup>Cn</sup>** ( $n=3, 12$ ) were prepared in three steps (Scheme 1). Ligand **L9**<sup>[15]</sup> was first transformed into the bis(tridentate)-



Scheme 1. Synthesis of ligands **L11** and **L12<sup>Cn</sup>** ( $n=3, 12$ ).

vinyl ether, followed by a quantitative thermal Claisen rearrangement to give **L11**.<sup>[14,16]</sup> The final thiol-ene click-coupling radical reactions provided **L12<sup>Cn</sup>** ( $n=3, 12$ ) in good yields.<sup>[17]</sup>

As previously established for **L9**,<sup>[15]</sup> the mixing of the more constrained ligand **L11** (3 equiv) with  $\text{Ln}(\text{OTf})_3 \cdot x\text{H}_2\text{O}$  (2 equiv;  $\text{Ln}=\text{La, Lu}$ ;  $\text{OTf}^- = \text{CF}_3\text{SO}_3^- = \text{triflate}$ ;  $x=1-3$ ) in aprotic solvent ( $\text{CH}_3\text{CN}$  or  $\text{DMSO}$ ) containing  $n\text{Bu}_4\text{NOH}$  (6 equiv) also yields orange solutions. ESI-MS spectra of the crude reaction solutions reveal weak signals corresponding to the formation of a small amount of protonated triple-helical complexes  $[\text{Ln}_2(\text{L11}-2\text{H})_3 + 2\text{H}]^{2+}$  ( $\text{Ln}=\text{La, Lu}$ , Figure S1 in the Supporting Information).<sup>[18]</sup> Because of the extreme energetic penalty accompanying the formation of the second intramolecular macrocyclization process with small cations,<sup>[15]</sup> the concomitant formation of the double-stranded helix  $[\text{Lu}_2(\text{L11}-2\text{H})_2 + 2\text{H}]^{2+}$  is detected for  $\text{Ln}=\text{Lu}$  (Figure S1 in the Supporting Information). For solubility reasons, the equilibrium shown in Equation (1) was monitored by  $^1\text{H}$  NMR spectroscopy in  $[\text{D}_6]\text{DMSO}$  ( $\text{Ln}=\text{La, Lu}$ ;  $k=9, 11$ ; Figure 1).



In line with previous thermodynamic studies,<sup>[15]</sup> the concomitant formation of double- and triple-stranded helicates for  $\text{Ln}=\text{Lu}$  produces very complicated spectra (Figure S2 in the Supporting Information), and we therefore focus on  $\text{Ln}=\text{La}$ , for which the larger stability constants ensure the exclusive formation of the triple-stranded helicate according to Equation (1) for a stoichiometric ratio  $\text{La}/\mathbf{Lk}=2:3$  and a total ligand concentration of 5 mM (Figure 1).<sup>[15]</sup> Both diamagnetic  $[\text{La}_2(\mathbf{Lk}-2\text{H})_3]$  complexes ( $k=9, 11$ ) display seven signals for the aromatic protons (Hb–Hh in Figure 1), which are diagnostic for either  $D_3$  (helical),  $C_{3h}$  (side-by-side = mesocate) or  $D_{3h}$  (nonhelical) point groups.<sup>[1c,d]</sup> The last nonhelical arrangement of the strands is discarded by the detection of pseudo-sextets ( $\text{ABX}_3$  spin systems for which  $^2J = 2 \cdot (^3J)$ ) for the diastereomeric methylene protons of the ethyl residues (Ho), while the singlet ( $A_2$  spin system) observed for the enantiotopic methylene protons (Ha) of the diphenylmethane spacer implies the existence of three twofold axes perpendicular to the threefold axis, which rules out the  $C_{3h}$  point group. We can thus safely conclude that the  $D_3$ -symmetrical triple-helical arrangement found for the non-substituted ligand strands in  $[\text{La}_2(\mathbf{L9}-2\text{H})_3]$  is preserved in  $[\text{La}_2(\mathbf{L11}-2\text{H})_3]$ . Interestingly, the equilibrium in Equation (1) offers the possibility to use the  $^1\text{H}$  NMR signals of the  $[n\text{Bu}_4\text{N}]^+$  ion as an internal reference. The comparison of the relative integration of the  $^1\text{H}$  NMR signals of the protons of the ligand bound to the complex with that of  $[n\text{Bu}_4\text{N}]^+$  indicates that the ligand is distributed between

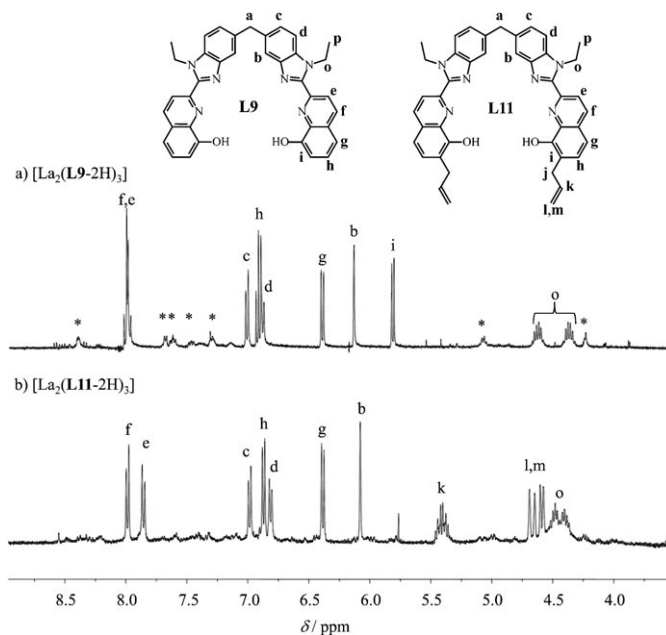


Figure 1.  $^1\text{H}$  NMR spectra with numbering scheme for the triple-stranded helicates a)  $[\text{La}_2(\mathbf{L9}-2\text{H})_3]$  and b)  $[\text{La}_2(\mathbf{L11}-2\text{H})_3]$  ( $[\text{D}_6]\text{DMSO}$ , 298 K, \* = free ligand).

$[\text{La}_2(\mathbf{L9}-2\text{H})_3]$  (80(5)% of ligand speciation) and  $[\mathbf{L9}-2\text{H}]^{2-}$  (20(5)% of the ligand speciation), in good agreement with predictions based on the experimental thermodynamic constants (Figure 1 a).<sup>[15]</sup> The situation is completely different for  $\mathbf{L11}$ , whereby the relative integration of the  $^1\text{H}$  NMR signals indicates that only 10(5)% of ligand speciation is involved in the formation of  $[\text{La}_2(\mathbf{L11}-2\text{H})_3]$ , while the remaining major part of the ligand was distributed between  $[\mathbf{L11}-2\text{H}]^{2-}$  (<5%) and what we tentatively ascribe to an intricate mixture of aggregates or polymers (85(10)%) in slow exchange on the NMR timescale (Figure 1 b).<sup>[19]</sup>

The application of the equilibrium in Equation (1) to  $\mathbf{L12}^{\text{C3}}$ , which contains additional thiopropyl residues (Scheme 1), leads to insoluble amorphous red solids, which could be filtered and then suspended in any solvent (>50 solvents or mixtures were investigated) without reaching the minimum solubility required for recording a reliable  $^1\text{H}$  NMR spectrum, except for the observation of the intense signals of the soluble  $[n\text{Bu}_4\text{N}]^+$  cation. Only ultrasensitive ESI-MS spectra of suspensions in acetonitrile showed very weak signals corresponding to traces of mono and diprotonated triple-helical complexes  $[\text{Ln}_2(\mathbf{L12}^{\text{C3}}-2\text{H})_3+\text{H}]^+$  and  $[\text{Ln}_2(\mathbf{L12}^{\text{C3}}-2\text{H})_3+2\text{H}]^{2+}$  in solution ( $\text{Ln}=\text{La}, \text{Eu}, \text{Lu}$ ). The insoluble red precipitates were washed with methanol in order to remove the soluble  $n\text{Bu}_4\text{NOTf}$  salt, and the subsequent elemental analyses of the dried solids were found to be compatible with  $[\text{Ln}_2(\mathbf{L12}^{\text{C3}}-2\text{H})_3]$  ( $\text{Ln}=\text{La}, \text{Eu}, \text{Lu}$ ) empirical formula (Table S1 in the Supporting Information). We thus conclude that the connection of axial alkyl residues of increasing length at the 7,7'-positions of the quinoline rings on going stepwise from  $\mathbf{L9}$  to  $\mathbf{L11}$  and  $\mathbf{L12}^{\text{C3}}$  destabilizes the formation of discrete helicates in favor of intricate mixtures of oligomeric and/or polymeric coordination aggregates in slow exchange, a phenomenon reminiscent of the modern concept of dynamic virtual combinatorial libraries (DVCL)<sup>[20]</sup> previously invoked during the formation of mixtures of polymeric complexes  $[\text{M}_2(\mathbf{L10}-2\text{H})_3]_\infty$  ( $\text{M}=\text{Al}, \text{Ga}, \text{Fe}, \text{Cr}$ ) obtained with a closely related bis-quinolinylate ligand.<sup>[14]</sup>

**Catching discrete neutral amphiphilic lanthanide triple-stranded helicates:** As often encountered in experimental science, some intuitions precede a rational and theoretically supported approach. Accordingly, we reasoned that the presence of six terminal polarizable double bonds in  $[\text{Ln}_2(\mathbf{L11}-2\text{H})_3]$  or six thioether substituents in  $[\text{Ln}_2(\mathbf{L12}^{\text{C3}}-2\text{H})_3]$  may contribute to the formation of intricate mixtures of oligomers and polymers as a consequence of nondirectional intra and intermolecular van der Waals interactions. We therefore selected  $\text{Ag}^{\text{I}}$ , a soft  $d^{10}$  spherical ion with no stereochemical preference, for interacting with the sulfur atoms at both ends of the helicates in order to force the self-organization of discrete helicates without competing with the lanthanide cations for the occupancy of the tridentate binding units.<sup>[21]</sup> Two equivalents of  $\text{AgOTf}$  were thus reacted with a suspension of each insoluble

$[\text{Ln}_2(\mathbf{L12}^{\text{C3}}-2\text{H})_3]$  ( $\text{Ln}=\text{La}, \text{Eu}, \text{Lu}$ ) polymeric complexes in organic solvents ( $\text{CH}_2\text{Cl}_2$ ,  $\text{CH}_3\text{OH}$ , or THF). Complete dissolution occurs, and leads to the exclusive detection of  $[\text{Ln}_2\text{Ag}_2(\mathbf{L12}^{\text{C3}}-2\text{H})_3]^{2+}$  ( $\text{Ln}=\text{La}, \text{Eu}, \text{Lu}$ ) by ESI-MS (Figure S3 in the Supporting Information). The  $^1\text{H}$  NMR spectra of these solutions show the quantitative formation (>95% ligand distribution) of a single complex displaying seven signals for the aromatic protons witnessing the existence of a threefold axis (Figure 2). The concomitant observation of a singlet for the enantiotopic methylene protons (Ho) of the diphenylmethane spacer and pseudo-sextets for the methylene protons (Hp) of the ethyl residues supports the putative formation of the discrete  $D_3$ -symmetrical triple-stranded helicates  $[\text{Ln}_2\text{Ag}_2(\mathbf{L12}^{\text{C3}}-2\text{H})_3]^{2+}$  ( $\text{Ln}=\text{La}, \text{Eu}, \text{Lu}$ ) in solution, in line with ESI-MS data.

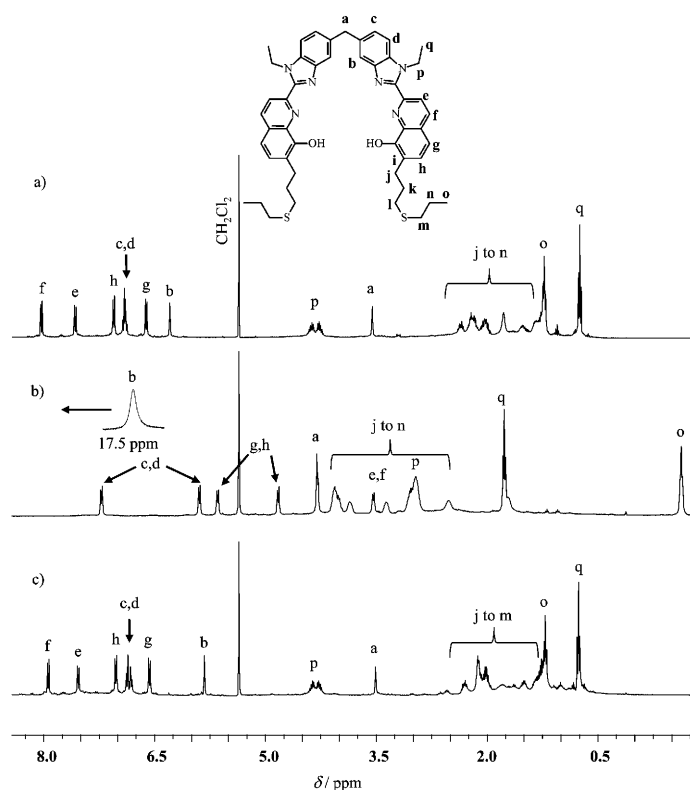


Figure 2.  $^1\text{H}$  NMR spectra with numbering scheme of the triple-stranded helicates a)  $[\text{La}_2\text{Ag}_2(\mathbf{L12}^{\text{C3}}-2\text{H})_3][\text{OTf}]_2$ , b)  $[\text{Eu}_2\text{Ag}_2(\mathbf{L12}^{\text{C3}}-2\text{H})_3][\text{OTf}]_2$  and c)  $[\text{Lu}_2\text{Ag}_2(\mathbf{L12}^{\text{C3}}-2\text{H})_3][\text{OTf}]_2$  ( $\text{CD}_2\text{Cl}_2$ , 298 K).

The molecular weights of a complex in solution ( $MM_C$ ) can be estimated by using Equation (2), in which  $D_C$  is its translational self-diffusion coefficient determined by NMR diffusion ordered spectroscopy (DOSY),  $\rho_C^{\text{H}}$  is the density of the complex, while  $MM_R = 497.5 \text{ g mol}^{-1}$ ,  $D_R$ , and  $\rho_R^{\text{H}}$  similarly stand for the reference compound  $n\text{Bu}_4\text{NOTf}$  (Appendix I).<sup>[22]</sup>

$$\frac{MM_C}{MM_R} = \left(\frac{D_R}{D_C}\right)^3 \frac{\rho_C^{\text{H}}}{\rho_R^{\text{H}}} \quad (2)$$

Assuming that the densities of the reference compound and of the lipophilic complexes are comparable ( $\rho_C^H/\rho_R^H \approx 1$ ), the application of Equation (2) to the experimental diffusion coefficients leads to  $MM_C^{\text{exptl}} = 3640$  (370)  $\text{g mol}^{-1}$  (Table S2 in the Supporting Information) in fair agreement with  $MM_C^{\text{calcd}} = 3255$ , 3281, and 3327  $\text{g mol}^{-1}$  calculated for  $[\text{Ln}_2\text{Ag}_2(\text{L12}^{\text{C}^3-2\text{H}})_3][\text{OTf}]_2$  with Ln=La, Eu, Lu, respectively. In modern language,<sup>[20]</sup> we can write that the addition of  $\text{Ag}^{\text{I}}$  to the dynamic combinatorial libraries produced by a mixture of  $\text{Ln}^{\text{III}}/[\text{L12}^{\text{C}^3-2\text{H}}]^{2-} = 2:3$  results in the stabilization of one specific complex to such an extent that it is expressed quantitatively in dichloromethane or methanol as the discrete assembly  $[\text{Ln}_2\text{Ag}_2(\text{L12}^{\text{C}^3-2\text{H}})_3][\text{OTf}]_2$ . Subsequent slow diffusion of diethyl ether into the deep red solutions of the each of the complexes in methanol yielded 80% of red crystals, which were dried under vacuum to give microcrystalline powders, the elemental analyses of which are compatible with  $[\text{Ln}_2\text{Ag}_2(\text{L12}^{\text{C}^3-2\text{H}})_3][\text{OTf}]_2 \cdot x\text{H}_2\text{O}$  (Table S1).

**Structure of the complex  $[\text{La}_2\text{Ag}_2(\text{L12}^{\text{C}^3-2\text{H}})_3][\text{OTf}]_2$  in the solid state:** Crystals of the lanthanum complexes were found to be suitable for X-ray analysis. The asymmetric unit contains one independent triple-stranded helical cation

$[\text{La}_2\text{Ag}_2(\text{L12}^{\text{C}^3-2\text{H}})_3]^{2+}$ , together with two anionic triflates and some interstitial solvent molecules in agreement with the global formula  $[\text{La}_2\text{Ag}_2(\text{L12}^{\text{C}^3-2\text{H}})_3][\text{OTf}]_2 \cdot 0.5\text{C}_4\text{H}_{10}\text{O} \cdot 0.5\text{CH}_3\text{OH}$  (1, Figure 3, and Tables S3–S5 in the Supporting Information). Each lanthanum atom is nine-coordinated by three head-to-head-to-head (HHH) helically wrapped tridentate binding units providing two terminal tripods, one formed by the three oxygen atoms of the phenolates ( $\text{O}_{\text{phenol}}$ ), and the second one containing the three nitrogen atoms of the benzimidazole rings ( $\text{N}_{\text{bzim}}$ ). Each rectangular face of the resulting pseudo-trigonal prism is capped by a nitrogen atom of a quinoline ring ( $\text{N}_{\text{quin}}$ , Figure 3 and Figure S4 in the Supporting Information). The La–O and La–N bond lengths (Table 1) are standard,<sup>[12]</sup> as confirmed by the computed bond valences  $\nu_{\text{La,donor}}$  (Table 1),<sup>[23]</sup> which compare well with those reported for the nonsubstituted reference triple-helical complex  $[\text{Nd}_2(\text{L9}-2\text{H})_3]$  (Table 1).<sup>[15]</sup> The La...La contact distance (8.9131(9) Å) is also close to that found for  $[\text{Nd}_2(\text{L9}-2\text{H})_3]$  (9.02–9.05 Å).<sup>[15]</sup> The thorough quantitative analysis of the geometry (Table S6 and Figure S4 in the Supporting Information), and of the helicity of dinuclear lanthanide core in  $[\text{La}_2\text{Ag}_2(\text{L12}^{\text{C}^3-2\text{H}})_3]^{2+}$  (Table S7 and Figure S5) shows no significant differences with those found for  $[\text{Nd}_2-$

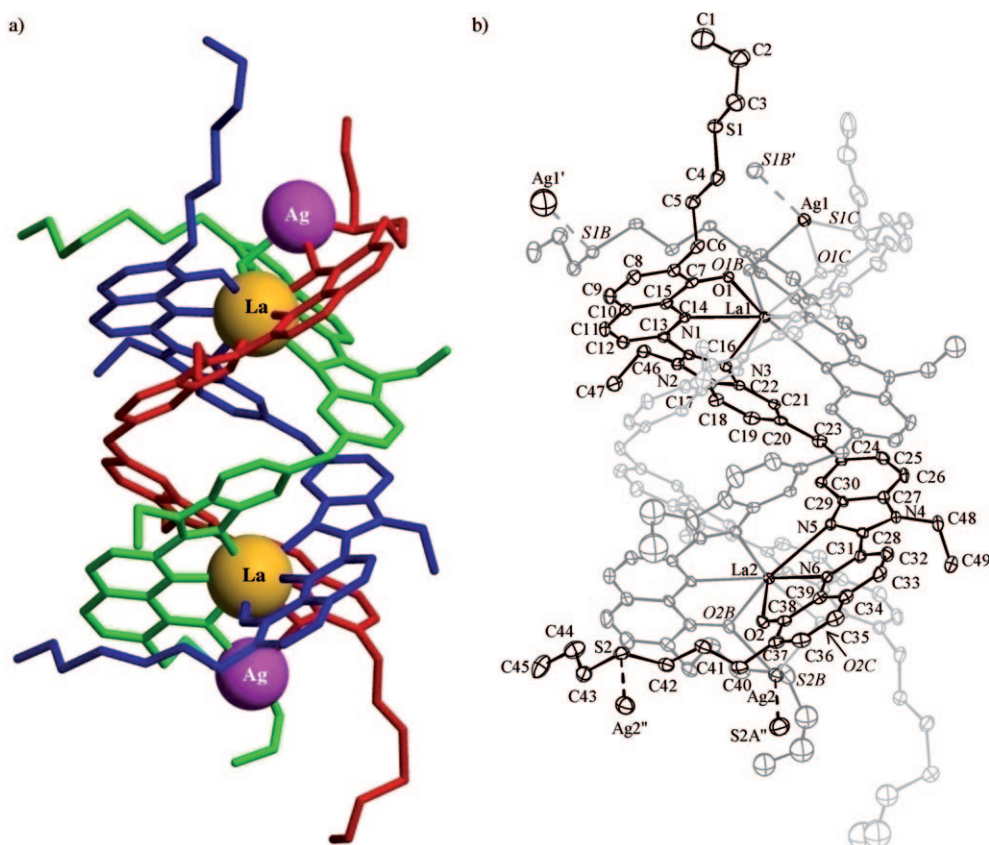


Figure 3. a) Perspective color view of the molecular structure of  $[\text{La}_2\text{Ag}_2(\text{L12}^{\text{C}^3-2\text{H}})_3]^{2+}$  approximately perpendicular to the pseudo-threefold helical axis (strand A: blue, strand B: green, strand C: red). b) Associated ORTEP view using different gray scale intensities for the strands and showing the numbering scheme for strand A. Ellipsoids are represented at 30% probability level. The solvent molecules, the ionic triflates anions and the hydrogen atoms have been omitted for clarity. The atoms numbered with italic fonts belong to strands B or C, while primed (or double-primed) atoms  $\text{Ag1}'$ ,  $\text{Ag2}''$ ,  $\text{S1B}'$  and  $\text{S2A}''$  belong to the neighboring complexes related by inversion centers.

Table 1.  $M \cdots <M>M$  distances, average M–N, M–O, and M–S distances, bond valences ( $\nu_{Mj}$ )<sup>[a]</sup> and bond valence sums ( $V_M$ )<sup>[b]</sup> in the crystal structure of  $[\text{La}_2\text{Ag}_2(\text{L12}^{\text{C}3}-2\text{H})_3]^{2+}$  and of related complexes.

	$[\text{La}_2\text{Ag}_2(\text{L12}^{\text{C}3}-2\text{H})_3]^{2+}$		A- $[\text{Nd}_2(\text{L9}-2\text{H})_3]$		B- $[\text{Nd}_2(\text{L9}-2\text{H})_3]$
	La1/Ag1	La2/Ag2	Nd2	Nd3	Nd1
Ln–N <sup>[bzim]</sup> <sup>[c]</sup> [Å]	2.78(3)	2.79(5)	2.72(6)	2.71(4)	2.73(3)
Ln–N <sup>[quin]</sup> <sup>[c]</sup> [Å]	2.72(3)	2.715(5)	2.66(3)	2.63(1)	2.65(1)
Ln–O <sup>[c]</sup> [Å]	2.46(1)	2.46(4)	2.41(1)	2.41(2)	2.39(1)
Ln $\cdots$ Ln [Å]	8.9131(9)	–	9.021(2)	–	9.047(2)
$\nu_{\text{Ln,N}(\text{bzim})}$ <sup>[c]</sup>	0.24(2)	0.24(3)	0.25(3)	0.25(3)	0.24(2)
$\nu_{\text{Ln,N}(\text{quin})}$ <sup>[c]</sup>	0.29(3)	0.294(4)	0.29(2)	0.314(8)	0.30(4)
$\nu_{\text{Ln,O}}$ <sup>[c]</sup>	0.43(1)	0.44(4)	0.413(6)	0.42(3)	0.44(5)
$V_{\text{Ln}}$	2.89	2.91	2.84	2.96	2.94
Ag–O <sup>[d]</sup> [Å]	2.4865(7)	2.5(1)	–	–	–
Ag–S <sup>[d]</sup> [Å]	2.481(8)	2.484(4)	–	–	–
Ag $\cdots$ Ag [Å]	15.559(2)	–	–	–	–
Ln $\cdots$ Ag <sup>[e]</sup> [Å]	3.7551(6)	3.7940(6)	–	–	–
$\nu_{\text{Ag,O}}$ <sup>[d]</sup>	0.14(3)	0.17(5)	–	–	–
$\nu_{\text{Ag,S}}$ <sup>[d]</sup>	0.376(9)	0.373(4)	–	–	–
$V_{\text{Ag}}$	1.02	1.09	–	–	–
reference	this work	this work	[15]	[15]	[15]

[a]  $\nu_{Mj} = e^{[(R_{Mj}-d_{Mj})/b]}$ , whereby  $d_{Mj}$  is the M–j (j=donor atom) distance. The valence bond parameters  $R_{\text{M,N}}$ ,  $R_{\text{M,O}}$  and  $R_{\text{M,Ag}}$  are taken from reference [23] and  $b=0.37$  Å. [b]  $V_M = \sum \nu_{Mj}$ .<sup>[23]</sup> [c,d] Each value is the average of three [c] or two [d] bond lengths and the numbers in brackets correspond to the standard deviations of the average values (the original uncertainties affecting each bond length are given in Table S4; bzim=benzimidazole and quin=quinoline). [e] Only the shortest intramolecular La $\cdots$ Ag distances are reported (La1 $\cdots$ Ag1 and La2 $\cdots$ Ag2).

( $\text{L9}-2\text{H})_3$ ].<sup>[15]</sup> We conclude that the axial substitution of thioalkyl groups in  $[\text{La}_2\text{Ag}_2(\text{L12}^{\text{C}3}-2\text{H})_3]^{2+}$  does not induce significant distortions within the dinuclear triple-stranded lanthanide-containing triple-helical portion, which can be thus almost perfectly superimposed with  $[\text{Nd}_2(\text{L9}-2\text{H})_3]$  (Figure S6).

The most striking feature in the crystal structure of **1** concerns the unsymmetrical coordination of the silver cations located at each extremity of the triple-stranded helical core. Each Ag atom is coordinated by two oxygen atoms of the phenolates (weak interactions, Table 1) and by two sulfur atoms of the thioether groups (strong interactions, Table 1). The four donor atoms contributing to the Ag coordination sphere adopt a highly distorted tetrahedral arrangement and belong to two different helical  $[\text{La}_2\text{Ag}_2(\text{L12}^{\text{C}3}-2\text{H})_3]^{2+}$  complexes related by an inversion centre, thus forming infinite linear coordination polymers along the  $[1\bar{1}\bar{1}]$  direction in the crystalline state (Figure 4 and Figure S7 in the Supporting Information). Two successive monomeric triple-helical cations within the polymeric chain are bridged by two intermolecular Ag–S bonds, while the two sulfur atoms S1A and

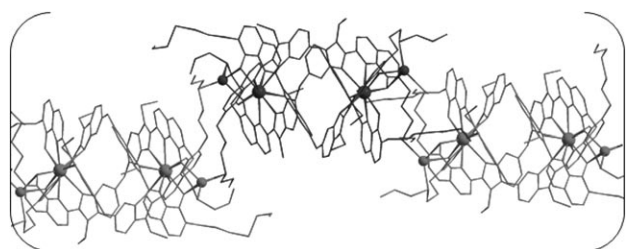


Figure 4. View of a segment (3 units) of the linear polymeric chains of  $[\text{La}_2\text{Ag}_2(\text{L12}^{\text{C}3}-2\text{H})_3]^{2+}$  perpendicular to the  $[1\bar{1}\bar{1}]$  direction.

S2C are not involved in the coordination with Ag<sup>I</sup>. The disymmetrical coordination of Ag<sup>I</sup> produces a severe distortion from pseudo-threefold symmetry for the global tetranuclear complexes

$[\text{La}_2\text{Ag}_2(\text{L12}^{\text{C}3}-2\text{H})_3]^{2+}$  with Ag1 (1.914(1) Å) and Ag2 (1.758(1) Å) being significantly remote from the La1 $\cdots$ La2 direction.

### Molecular dynamics for reconciling the solid-state and the solution structures of $[\text{Ln}_2\text{Ag}_2(\text{L12}^{\text{C}3}-2\text{H})_3][\text{OTf}]_2$ :

The  $D_3$ -symmetrical structure evidenced in solution by NMR spectroscopy for  $[\text{La}_2\text{Ag}_2(\text{L12}^{\text{C}3}-2\text{H})_3]^{2+}$  contrasts with the polymeric organization found in the crystalline state, in which the silver cations are un-

symmetrically bound to sulfur and oxygen atoms. To reconcile these two patterns, we performed MD simulations in the gas phase and in  $\text{CH}_2\text{Cl}_2$ . A first 20 ns MD gas phase simulation of  $[\text{La}_2\text{Ag}_2(\text{L12}^{\text{C}3}-2\text{H})_3]^{2+}$  performed after a preliminary energy minimization of the structure, indicates that the complex exists as a discrete entity, but its overall triple-helical shape remains globally unchanged (Figure 5a). The flexible terminal thioalkyl side chains are curled up as a direct consequence of the in vacuo model, which prevents significant dispersion of the aliphatic chains. Except for a slight lengthening of the La–O<sub>phenol</sub> bonds, the geometrical characteristics of the gas phase simulated lanthanide-containing triple-stranded helical core in  $[\text{La}_2\text{Ag}_2(\text{L12}^{\text{C}3}-2\text{H})_3]^{2+}$  (Table 2 and Table S8 in the Supporting Information) closely resemble those found in the solid state (Table 1 and Table S4 in the Supporting Information).

The crucial difference arises from the removal of any significant Ag–O<sub>phenol</sub> interaction in the gas phase (Figures S8 and S9 in the Supporting Information), while the MD simulations show that merely two Ag–S bonds (criterion for Ag–S bonding  $< 4$  Å) can simultaneously exist in the gas phase (Figure 6a and Figure S10 in the Supporting Information). Each silver cation cannot simultaneously be involved in three Ag–S bonds; however, the bound sulfur atoms are regularly exchanged during the 20 ns simulation, thus producing a highly dynamic and evenly balanced coordination sphere around Ag<sup>I</sup>. The average total time during which each Ag–S distance is shorter than 4 Å during the 20 ns of the MD simulation in the gas phase amounts to 16.8 ns per sulfur atom. Assuming that 1) a sulfur atom that spends 20 ns coordinated to Ag<sup>I</sup> contributes a value of 1 to the coordination number (CN) and 2) there are six sulfur atoms

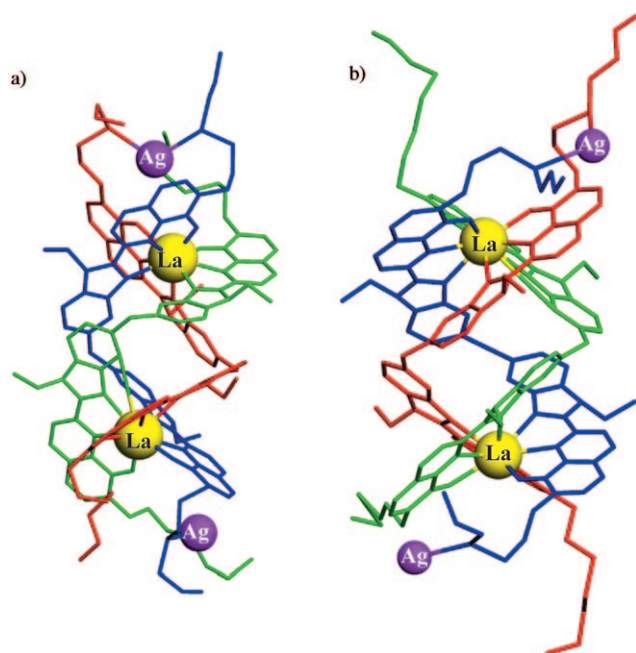


Figure 5. Optimized structures of  $[\text{La}_2\text{Ag}_2(\text{L12}^{\text{C}3}-2\text{H})_3]^{2+}$  after 15 ns MD simulation, a) in the gas phase and b) in  $\text{CH}_2\text{Cl}_2$ , highlighting the effect of solvent on the peripheral alkyl chains.

Table 2.  $\text{La}\cdots\text{La}$  distances, average  $\text{La}-\text{N}$  and  $\text{La}-\text{O}$  distances, bond valences ( $\nu_{\text{La},j}$ )<sup>[a]</sup> and bond valence sums ( $V_{\text{La}}$ )<sup>[b]</sup> in  $[\text{La}_2\text{Ag}_2(\text{L12}^{\text{C}3}-2\text{H})_3]^{2+}$  simulated by MD (20 ns) in the gas phase and in  $\text{CH}_2\text{Cl}_2$ .

	Gas phase		Solution	
	La1	La2	La1	La2
$\text{La}-\text{N}_{\text{bzim}}^{[\text{c}]} [\text{\AA}]$	2.79(4)	2.79(4)	2.82(1)	2.82(2)
$\text{La}-\text{N}_{\text{quin}}^{[\text{c}]} [\text{\AA}]$	2.75(2)	2.76(2)	2.77(1)	2.77(1)
$\text{La}-\text{O}^{[\text{c}]} [\text{\AA}]$	2.57(2)	2.56(3)	2.58(0)	2.57(1)
$\text{La}\cdots\text{La} [\text{\AA}]$	10.0(2)	–	9.8(3)	–
$\nu_{\text{La},\text{N}(\text{bzim})}^{[\text{c}]}$	0.24(3)	0.24(3)	0.223(9)	0.26(1)
$\nu_{\text{La},\text{N}(\text{quin})}^{[\text{c}]}$	0.27(1)	0.26(1)	0.257(4)	0.250(8)
$\nu_{\text{La},\text{O}}^{[\text{c}]}$	0.32(2)	0.33(3)	0.31(1)	0.32(1)
$V_{\text{La}}$	2.48	2.49	2.37	2.38

[a]  $\nu_{\text{La},j} = e^{[(R_{\text{La},j}-d_{\text{La},j})/b]}$ , whereby  $d_{\text{La},j}$  is the  $\text{La}-j$  ( $j = \text{donor atom}$ ) distance. The valence bond parameters  $R_{\text{La},\text{N}}$  and  $R_{\text{La},\text{O}}$  are taken from ref. 23 and  $b = 0.37 \text{ \AA}$ . [b]  $V_{\text{La}} = \sum \nu_{\text{La},j}$ .<sup>[23]</sup> Though the latter parameters are only valid for solid-state structures, we compute similar data for MD simulations in the gas phase and in solution for comparison purpose. [c] Each value is the average of three bond lengths and the number in brackets corresponds to the standard deviation of the average (the original uncertainties affecting each bond length are given in Table S8 Supporting Information; bzim = benzimidazole and quin = quinoline).

accessible to two  $\text{Ag}^{\text{I}}$  in the complex, we easily deduce an average coordination number per silver cation of  $CN = [(16.8 \times 6)/20]/2 = 2.5$ . Performing the same MD simulation for  $[\text{La}_2\text{Ag}_2(\text{L12}^{\text{C}3}-2\text{H})_3]^{2+}$  within a box of explicit dichloromethane molecules for modeling the solvent (see Experimental Section) leads to globally similar results as those found in the gas phase (Table 2 and Figure 6b; and Figure S11–S13 and Table S8 in the Supporting Information).

Solvent effects are however easily identified, since the bond-valences  $\nu_{\text{La},\text{donor}}$  and bond-valence sum  $V_{\text{La}}$  for each  $\text{La}^{\text{III}}$  are significantly reduced (Table 2). Moreover, the thio-

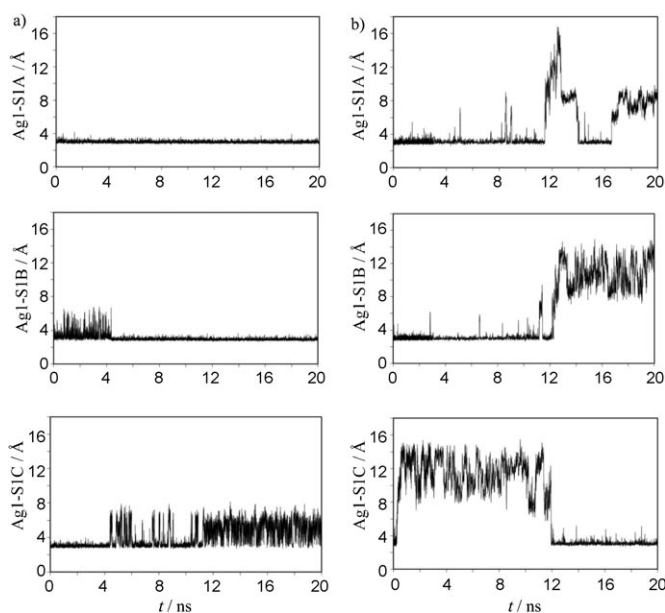


Figure 6. Variation in  $\text{Ag1}-\text{Sn}$  ( $n = 1\text{A}, 1\text{B}$  and  $1\text{C}$ ) distances  $[\text{\AA}]$  for  $[\text{La}_2\text{Ag}_2(\text{L12}^{\text{C}3}-2\text{H})_3]^{2+}$  a) in the gas phase and b) in  $\text{CH}_2\text{Cl}_2$  during the 20 ns of the MD simulations.

alkyl chains are now solvated by  $\text{CH}_2\text{Cl}_2$  and adopt extended conformations (Figure 5 b), which induce larger amplitudes for the  $\text{Ag}-\text{S}$  distances. Again, the coordination sphere around  $\text{Ag}^{\text{I}}$  is highly dynamic in  $\text{CH}_2\text{Cl}_2$ , and we calculate an average coordination number of  $CN = 1.5$  from the 20 ns MD simulation. Since the timescale of sulfur exchange process in solution is at least 3–5 orders of magnitude faster than the typical  $^1\text{H}$  NMR millisecond timescale, we conclude that the average  $D_3$ -symmetry observed by  $^1\text{H}$  NMR spectroscopy for  $[\text{La}_2\text{Ag}_2(\text{L12}^{\text{C}3}-2\text{H})_3]^{2+}$  in solution corresponds to a dynamic dimetallic tetranuclear triple-stranded helicates, in which the  $\text{Ag}^{\text{I}}$  are located on the helical axis and coordinated to three fast interchanging sulfur atoms.<sup>[24]</sup> Finally, the building of the Connolly surface<sup>[25]</sup> around the simulated structure of  $[\text{La}_2\text{Ag}_2(\text{L12}^{\text{C}3}-2\text{H})_3]^{2+}$  in  $\text{CH}_2\text{Cl}_2$  (Figure S15 in the Supporting Information) leads to an estimation of its molecular volume in solution ( $V_{\text{C}}^{\text{mol}} = 3324 \text{ \AA}^3$ ), which closely matches the experimental pseudo-spherical hydrodynamic volume determined by DOSY-NMR spectroscopy in  $\text{CD}_2\text{Cl}_2$  ( $V_{\text{C}}^{\text{H}} = 2855(195) \text{ \AA}^3$ , Table S2 in the Supporting Information), in line with a globular behavior of this nanometric object in solution.<sup>[22d]</sup>

**Toward an inductive approach for the stabilization of amphiphilic dinuclear lanthanide triple-stranded helicates with flexible axial substituents:** Despite the connection of six linear 4-thioheptyl chains, neither the polymeric insoluble complexes  $[\text{Ln}_2(\text{L12}^{\text{C}3}-2\text{H})_3]_{\infty}$ , nor its discrete derivative  $[\text{La}_2\text{Ag}_2(\text{L12}^{\text{C}3}-2\text{H})_3][\text{OTf}]_2$  display thermotropic liquid crystalline properties, which points to an insufficient micro-segregation induced by these amphiphilic molecules. To circumvent this limitation, a common strategy in material science relies on the systematic extension of the alkyl chains.<sup>[10]</sup>

MD simulations were then performed for  $[\text{La}_2\text{Ag}_2(\text{L12}^{Cn}-2\text{H})_3]^{2+}$  grafted with alkyl chains of increasing length ( $n=1, 3, 6, 9, 12$ ). In all cases, the dinuclear triple-helical lanthanide core remains intact in the gas phase and in  $\text{CH}_2\text{Cl}_2$  during the 20 ns simulation. The only significant changes concern the stepwise increase of the  $\text{La}-\text{O}_{\text{phenol}}$  bond lengths associated with the steric bulk produced by longer alkyl chains (Figure 7 and Table S9 in the Supporting Information). Along the complete series  $[\text{La}_2\text{Ag}_2(\text{L12}^{Cn}-2\text{H})_3]^{2+}$  ( $n=1, 3, 6, 9, 12$ ), no significant  $\text{Ag}-\text{O}_{\text{phenol}}$  interaction could be evidenced by MD (Figure S16 and S17 in the Supporting Information), while  $\text{Ag}-\text{S}$  close contact distances ( $<4 \text{ \AA}$  considered as bonding interactions) are systematically observed in the gas phase (Fig-



Figure 7. Optimized structures of  $[\text{La}_2\text{Ag}_2(\text{L12}^{C12}-2\text{H})_3]^{2+}$  obtained by MD simulations, a) in the gas phase (20 ns) and b) in  $\text{CH}_2\text{Cl}_2$  (5 ns) highlighting the effect of solvent on the conformation of the peripheral alkyl chains.

ure 8a and Figure S18 in the Supporting Information) despite the increasing bulk of the  $\text{Ag}^I$  coordination sphere with longer terminal alkyl chains.

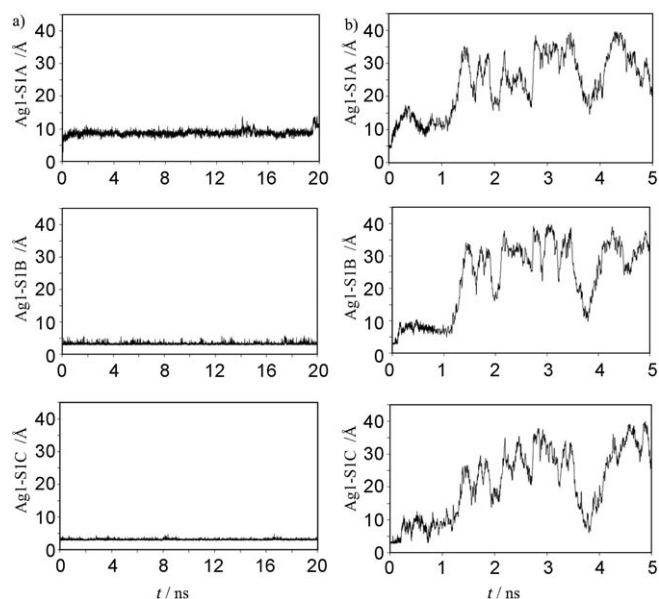


Figure 8. Variation in  $\text{Ag1-Sn}$  ( $n=1\text{A}, 1\text{B}$  and  $1\text{C}$ ) distances [ $\text{\AA}$ ] for  $[\text{La}_2\text{Ag}_2(\text{L12}^{C12}-2\text{H})_3]^{2+}$  a) in the gas phase (20 ns) and b) in  $\text{CH}_2\text{Cl}_2$  (5 ns) during the MD simulations.

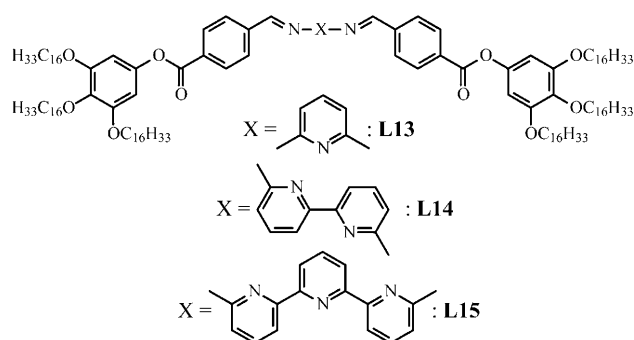
Contrary to the behavior found for  $[\text{La}_2\text{Ag}_2(\text{L12}^{C3}-2\text{H})_3]^{2+}$  (Figure 6), the unbound sulfur atom for  $n=6, 9$ , and  $12$ , do not oscillate between bound and non-bound positions and remain distant ( $8 \text{ \AA}$ ) from the silver cations in  $[\text{La}_2\text{Ag}_2(\text{L12}^{Cn}-2\text{H})_3]^{2+}$  (Figure 8a and Figure S8 in the Supporting Information). The two remaining sulfur atoms that interact with  $\text{Ag}^I$ , lie in the coordination sphere during the complete gas-phase MD simulation. The slowing down of the dynamic exchange for the thioether groups around  $\text{Ag}^I$  results from the considerable energy needed to move and rearrange long aliphatic chains, which are tightly packed in the gas phase. In  $\text{CH}_2\text{Cl}_2$ , in which the flexible alkyl chains are efficiently solvated and adopt extended conformation (Figure 7b), MD simulations show that for  $n=6, 9$ , and  $12$ , the  $\text{Ag}^I$  ions once and for all leave the complex during the first nanosecond and stay in the bulk solution (Figure 8b and Figure S19 in the Supporting Information). We deduce that the favorable interaction of the sulfur atoms with the electrostatic potential of the silver cation is obtained at the cost of some loss in solvation of the alkyl chains in  $\text{CH}_2\text{Cl}_2$ . For small chains in  $[\text{La}_2\text{Ag}_2(\text{L12}^{Cn}-2\text{H})_3]^{2+}$  ( $n=1-3$ ), the energetic penalty brought by incomplete solvation is small enough to quantitatively form discrete dimetallic helical complex in solution upon addition of  $\text{Ag}^I$ . For ( $n=6-12$ ), MD predicts that  $\text{Ag}^I$  is not able to efficiently interact with  $[\text{La}_2(\text{L12}^{Cn}-2\text{H})_3]$  to form  $[\text{La}_2\text{Ag}_2(\text{L12}^{Cn}-2\text{H})_3]^{2+}$  as a stable complex in solution. Indeed, the experiment confirms this prediction. We

treated ligand **L12**<sup>C12</sup> (3 equiv) with La(OTf)<sub>3</sub>·3H<sub>2</sub>O (2 equiv) in aprotic CH<sub>2</sub>Cl<sub>2</sub>/CH<sub>3</sub>CN mixture containing *n*Bu<sub>4</sub>NOH (6 equiv) according to the equilibrium given in Equation (1). As previously described for [La<sub>2</sub>(**L12**<sup>C3</sup>-2H)<sub>3</sub>], a red precipitate is readily formed. Evaporation to dryness followed by complete redissolving in pure dichloromethane gives a clear red solution, the <sup>1</sup>H NMR spectrum of which at any accessible temperature shows some well-resolved signals for the [*n*Bu<sub>4</sub>N]<sup>+</sup> ion, but only very weak and broad signals for the protons of the complexed ligands. This is compatible with the formation of an intricate mixture of soluble, but slow exchanging oligomers and polymers in solution (Figure 9a and Figure S20 in the Supporting Information). The addition of a stoichiometric amount of AgOTf (2 equiv) into the solution slightly improves the situation with the emergence of well-resolved <sup>1</sup>H NMR signals (Figure 9b), which witness the formation of the discrete D<sub>3</sub>-symmetrical triple-stranded helicate [La<sub>2</sub>Ag<sub>2</sub>(**L12**<sup>C12</sup>-2H)<sub>3</sub>]<sup>2+</sup>. The associated ESI-MS spectrum unambiguously confirms the formation of [La<sub>2</sub>Ag<sub>2</sub>(**L12**<sup>C12</sup>-2H)<sub>3</sub>]<sup>2+</sup> as the only cationic species formed in significant quantity (Figure S21 in the Supporting Information). However, when [La<sub>2</sub>Ag<sub>2</sub>(**L12**<sup>C3</sup>-2H)<sub>3</sub>]<sup>2+</sup> is quantitatively obtained in solution at millimolar concentration in CD<sub>2</sub>Cl<sub>2</sub>, the integration of the <sup>1</sup>H NMR spectrum indicates that only 25% of the ligand speciation contributes to the formation of [La<sub>2</sub>Ag<sub>2</sub>(**L12**<sup>C12</sup>-2H)<sub>3</sub>]<sup>2+</sup> in solution, while the remaining 75% contributes to the background mixture of uncharacterized polymers. As inferred from MD simula-

tions, we conclude that the use of Ag<sup>I</sup> as a bait for extracting these discrete nanometric lanthanide complexes from the mother polymeric mixture is indeed limited to thioether with short alkyl chains.

## Conclusion

As previously described by Douce, Ziesel, and co-workers in their pioneering work dedicated to the design of the amphiphilic double-stranded helicates [Cu<sub>2</sub>(**Lk**)<sub>2</sub>][BF<sub>4</sub>]<sub>2</sub> (*k* = 13–15) displaying (lamello)columnar mesomorphism, the con-



nection of long alkyl chains at the termini of the ligand strand severely limits the stability of the final complexes.<sup>[26]</sup> This effect is even more dramatic for the triple-stranded helicates [Ln<sub>2</sub>(**L12**<sup>C*n*</sup>-2H)<sub>3</sub>] (*n* = 3, 12), for which the axial connection of flexible thioalkyl chains produces intricate and poorly soluble mixtures of complexes displaying broad <sup>1</sup>H NMR spectra, a behavior indicative of mixtures of slowly exchanging hybrid oligomers/polymers.

The addition of Ag<sup>I</sup> has beneficial consequences in transforming the noncontrolled van der Waals interactions brought by the flexible chains into some specific and directional Ag–S interactions. The dimetallic tetranuclear triple-stranded helicates [Ln<sub>2</sub>Ag<sub>2</sub>(**L12**<sup>C3</sup>-2H)<sub>3</sub>]<sup>2+</sup> can be thus obtained quantitatively at millimolar concentration, and further crystallized in good yield. Interestingly, the crystalline structure shows the formation of a linear polymeric chains, in which the neutral triple-stranded cores [La<sub>2</sub>(**L12**<sup>C3</sup>-2H)<sub>3</sub>] are connected along the [111] direction by coordinated Ag<sup>I</sup> cations. In solution, the higher average D<sub>3</sub>-symmetry found for the discrete complexes [Ln<sub>2</sub>Ag<sub>2</sub>(**L12**<sup>C3</sup>-2H)<sub>3</sub>]<sup>2+</sup> results from fast exchange of the coordinating sulfur atoms. In this context, MD performed in the gas phase and in explicit solvent proved to be a useful tool for predicting and rationalizing the nature of the Ag–S interactions. Due to the less favorable energetic balance predicted by MD for approaching longer chains, the same ‘fishing’ procedure applied to 4-thiohexaalkyl chains in [Ln<sub>2</sub>(**L12**<sup>C12</sup>-2H)<sub>3</sub>] only gives 25% of [Ln<sub>2</sub>Ag<sub>2</sub>(**L12**<sup>C12</sup>-2H)<sub>3</sub>]<sup>2+</sup> in solution as measured by <sup>1</sup>H NMR spectroscopy; the major part of the ligand distribution remaining in the form of slow exchanging polymers.

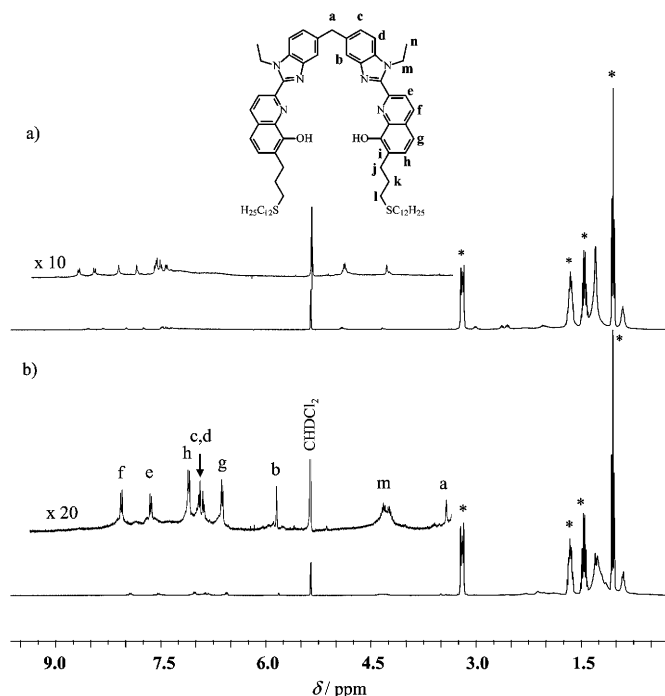


Figure 9. <sup>1</sup>H NMR spectra with numbering scheme of a) the mother polymeric mixture of [La<sub>2</sub>(**L12**<sup>C12</sup>-2H)<sub>3</sub>] and b) after treatment with AgOTf (2 equiv) indicating the formation of [La<sub>2</sub>Ag<sub>2</sub>(**L12**<sup>C12</sup>-2H)<sub>3</sub>]<sup>2+</sup> (CD<sub>2</sub>Cl<sub>2</sub>, 298 K, \* = signal of [*n*Bu<sub>4</sub>N]<sup>+</sup>).

With this predictive approach at hand, we screened several monovalent cations exhibiting potential interactions with the sulfur atoms of the side chains. By experiment, we found no templating activity for hard alkaline cations ( $M = \text{Li}^+$ ,  $\text{Na}^+$  and  $\text{K}^+$ ), while the softer  $\text{Cu}^{\text{I}}$  cation produces only faint ESI-MS motives compatible with its incorporation within the lanthanide helical complexes (Figure S22a in the Supporting Information). Interestingly, MD simulation suggested some favorable interactions with  $\text{Tl}^{\text{I}}$ , but weaker than those theoretically simulated for  $\text{Ag}^{\text{I}}$ . Experimentally, we indeed observed the partial extraction of  $[\text{La}_2\text{Tl}_2(\text{L12}^{\text{C3}}-2\text{H})_3]^{2+}$  from the reaction of  $[\text{La}_2(\text{L12}^{\text{C3}}-2\text{H})_3]$  with  $\text{TlOTf}$  (ESI-MS, Figure S22b), but in negligible proportions ( $^1\text{H NMR}$  spectroscopy) compared with the same procedure using  $\text{Ag}^{\text{I}}$  (Figure 9 and Figure S22c in the Supporting Information). Although the ultimate goal of producing molecular interfaces perpendicular to the helical axis in the amphiphilic lanthanide-containing triple-stranded helicates  $[\text{Ln}_2(\text{L12}^{\text{C12}}-2\text{H})_3]$  only partially succeeded, the strategy of using  $\text{Ag}^{\text{I}}$  as a bait for soft sulfur atoms introduced by a simple click thiol-ene radical reaction into the long flexible alkyl chains, proved to be valid providing that geometrical parameters are adapted to maximize the favorable enthalpic contribution brought by this extra complexation process. Further work along these lines will take advantage of predictive MD simulations for optimizing the position of the sulfur atom within the chain with respect to the best templating cation.

## Experimental Section

**General:** Chemicals were purchased from Acros, Alfa Aesar, and Aldrich, and used without further purification unless otherwise stated. The trifluoromethanesulfonate salts  $\text{Ln}(\text{CF}_3\text{SO}_3)_3 \cdot x\text{H}_2\text{O}$  were prepared from the corresponding oxide (Aldrich, 99.99%)<sup>[27]</sup> The Ln contents of solid salts were determined by complexometric titrations with Titriplex III (Merck) in the presence of urotropine and xylene orange.<sup>[28]</sup> Acetonitrile and dichloromethane were distilled over calcium hydride. Methanol was distilled over  $\text{Mg}(\text{OCH}_3)_2$ . Silica gel plates Merck 60 F254 were used for thin layer chromatography (TLC) and Fluka silica gel 60 (0.04–0.063 mm) was used for preparative column chromatography. The ligand **L9** was prepared according to literature.<sup>[15]</sup>

**Preparation of bis(tridentate)vinyl ether:** Anhydrous  $\text{K}_2\text{CO}_3$  (1.87 g, 13.50 mmol) and a catalytic amount of KI (100 mg) were added to a solution of **L9** (0.80 g, 1.35 mmol) and 3-chloropropene (0.83 g, 10.80 mmol) in acetone (200 mL). The reaction mixture was stirred at 70 °C for two days under a nitrogen atmosphere. The reaction mixture was evaporated to dryness and the resulting yellow solid was partitioned between  $\text{CH}_2\text{Cl}_2/\text{H}_2\text{O}$  (100 mL:100 mL). The aqueous phase was separated, then extracted with  $\text{CH}_2\text{Cl}_2$  (3 × 150 mL). The organic layers were gathered, dried over anhydrous  $\text{MgSO}_4$ , filtered and evaporated to dryness. The product was purified by column chromatography (silica gel (120 g),  $\text{CH}_2\text{Cl}_2/\text{MeOH}$  100:0→98:2) to yield 0.72 g (1.07 mmol, yield: 80%) of bis(tridentate)vinyl ether as a yellow solid.  $^1\text{H NMR}$  (400 MHz,  $\text{CDCl}_3$ ):  $\delta = 1.62$  (t,  $^3J = 6.9$  Hz, 6H), 4.34 (s, 2H), 4.81 (d,  $^3J = 5.5$  Hz, 4H), 5.15 (q,  $^3J = 6.9$  Hz, 4H), 5.40 (m, 2H), 5.56 (m, 2H), 6.21–6.31 (m, 2H), 7.12 (dd,  $^3J = 7.5$  Hz, 4J = 1.2 Hz, 2H), 7.29 (dd,  $^3J = 7.5$  Hz, 4J = 1.2 Hz, 2H), 7.41–7.53 (6H, m), 7.79 (2H, s), 8.25 (d,  $^3J = 8.8$  Hz, 2H), 8.61 ppm (d,  $^3J = 8.8$  Hz, 2H); ESIMS ( $\text{CH}_2\text{Cl}_2/\text{MeOH}$  9:1):  $m/z$ : 671.8  $[\text{M}+\text{H}]^+$ , 1342.6  $[2\text{M}+\text{H}]^+$ , 2013.4  $[3\text{M}+\text{H}]^+$ .

**Preparation of L11:** Bis(tridentate)vinyl ether (0.20 g, 0.30 mmol) was heated at 170 °C under an inert atmosphere for 12 h in absence of solvent to give 0.20 g (0.30 mmol, yield: 100%) of **L11** as a gray-brown solid.  $^1\text{H NMR}$  (400 MHz,  $\text{CDCl}_3$ ):  $\delta = 1.71$  (t,  $^3J = 7.1$  Hz, 6H), 3.69 (dt,  $^3J = 6.5$  Hz, 4J = 1.5 Hz, 4H), 4.35 (s, 2H), 4.90 (q,  $^3J = 7.1$  Hz, 4H), 5.13–5.21 (m, 4H), 6.08–6.18 (m, 2H), 7.32 (dd,  $^3J = 8.4$  Hz, 4J = 1.6 Hz, 2H), 7.39 (d,  $^3J = 8.4$  Hz, 2H), 7.43 (d,  $^3J = 8.4$  Hz, 2H), 7.44 (d,  $^3J = 8.4$  Hz, 2H), 7.79 (2H, s), 8.00 (2H, s), 8.29 (d,  $^3J = 8.7$  Hz, 2H), 8.55 ppm (d,  $^3J = 8.7$  Hz, 2H); ESIMS ( $\text{CH}_2\text{Cl}_2/\text{MeOH}$  9:1):  $m/z$ : 671.8  $[\text{M}+\text{H}]^+$ , 1342.6  $[2\text{M}+\text{H}]^+$ ; elemental analysis calcd (%) for  $\text{C}_{43}\text{H}_{38}\text{N}_6\text{O}_2 \cdot 0.38\text{H}_2\text{O}$ : C 76.22, H 5.77, N 12.40; found: C 76.25, H 5.55, N 12.11.

**Preparation of L12<sup>C3</sup>:** Finely ground ligand **L11** (0.154 g, 0.23 mmol) was suspended in dioxane (2 mL) and a large excess of 1-propanethiol (2 mL) was added. The reaction mixture was heated at 75 °C under a nitrogen atmosphere, and a catalytic quantity of azobisisobutyronitrile (AIBN; 5 mg) was added. After 4 h., 5 mg more AIBN were added. After a total reaction time of 12 h, the starting product was entirely consumed (TLC:  $\text{CH}_2\text{Cl}_2/\text{MeOH}$  95:5). The solution was evaporated to dryness and the resulting yellow solid was dried under vacuum. The crude product was purified by column chromatography (silica gel (50 g),  $\text{CH}_2\text{Cl}_2/\text{MeOH}$  100:0→99:1). Slow evaporation of the isolated amorphous solid in  $\text{CH}_2\text{Cl}_2/\text{MeOH}$  (12.5 mL:12.5 mL) gave pale yellow crystals **L12<sup>C3</sup>**, which were filtered, washed with cold MeOH and dried under vacuum (0.135 g, 0.17 mmol, yield: 76%).  $^1\text{H NMR}$  (400 MHz,  $\text{CDCl}_3$ ):  $\delta = 1.01$  (t,  $^3J = 7.3$  Hz, 6H), 1.64 (sext,  $^3J = 7.4$  Hz, 4H), 1.72 (t,  $^3J = 7.1$  Hz, 6H), 2.07 (q,  $^3J = 7.4$  Hz, 4H), 2.55 (t,  $^3J = 7.4$  Hz, 4H), 2.64 (t,  $^3J = 7.4$  Hz, 4H), 3.02 (t,  $^3J = 7.4$  Hz, 4H), 4.35 (s, 2H), 4.90 (q,  $^3J = 7.3$  Hz, 4H), 7.30–7.47 (m, 8H), 7.80 (s, 2H), 7.99 (s, 2H), 8.29 (d,  $^3J = 8.6$  Hz, 2H), 8.54 ppm (d,  $^3J = 8.6$  Hz, 2H);  $^{13}\text{C NMR}$  (100 MHz,  $\text{CDCl}_3$ ):  $\delta = 13.55$ , 15.43, 23.03, 29.21, 29.76, 31.76, 34.21, 40.77, 42.25, 109.89, 117.54, 120.27, 122.03, 124.24, 125.36, 126.49, 130.55, 134.94, 136.67, 136.75, 137.06, 143.08, 148.19, 149.22, 149.26 ppm; ESIMS ( $\text{CH}_2\text{Cl}_2/\text{MeOH}$  9:1):  $m/z$ : 824.1  $[\text{M}+\text{H}]^+$ , 1647.3  $[2\text{M}+\text{H}]^+$ ; elemental analysis calcd (%) for  $\text{C}_{49}\text{H}_{54}\text{N}_6\text{O}_2 \cdot 1.66\text{H}_2\text{O}$ : C 68.99, H 6.77, N 9.85; found: C 68.98, H 6.46, N 9.77.

**Preparation of L12<sup>C12</sup>:** Finely ground ligand **L11** (0.10 g,  $1.49 \times 10^{-4}$  mol) was suspended in dioxane (1 mL) and a large excess of 1-propanethiol (1 mL) was added. The reaction mixture was heated at 75 °C under a nitrogen atmosphere, and a catalytic quantity of AIBN (5 mg) was added. After 4 h., 5 mg more AIBN were added. After a total reaction time of 12 h, the entire starting product was consumed (TLC:  $\text{CH}_2\text{Cl}_2/\text{MeOH}$  95:5). The solution was evaporated to dryness and the resulting yellow waxy solid was dried under vacuum. The crude product was purified by column chromatography (silica gel (50 g),  $\text{CH}_2\text{Cl}_2/\text{MeOH}$  100:0→99:1) to yield 0.12 g ( $1.12 \times 10^{-4}$  mol, yield: 75%) of **L12<sup>C12</sup>** as a yellow solid.  $^1\text{H NMR}$  (400 MHz,  $\text{CDCl}_3$ ):  $\delta = 0.90$  (t,  $^3J = 7.0$  Hz, 6H), 1.22–1.45 (m, 36H), 1.61 (quint,  $^3J = 7.4$  Hz, 4H), 1.72 (t,  $^3J = 7.2$  Hz, 4H), 2.07 (quint,  $^3J = 7.4$  Hz, 4H), 2.56 (t,  $^3J = 7.4$  Hz, 4H), 2.64 (t,  $^3J = 7.4$  Hz, 4H), 3.02 (t,  $^3J = 7.4$  Hz, 4H), 4.35 (s, 2H), 4.90 (q,  $^3J = 7.2$  Hz, 4H), 7.31 (dd,  $^3J = 8.5$  Hz, 4J = 1.4 Hz, 2H), 7.38 (d,  $^3J = 7.4$  Hz, 2H), 7.41–7.47 (m, 4H), 7.79 (s, 2H), 7.98 (s, 2H), 8.29 (d,  $^3J = 8.7$  Hz, 2H), 8.54 ppm (d,  $^3J = 8.7$  Hz, 2H);  $^{13}\text{C NMR}$  (100 MHz,  $\text{CDCl}_3$ ):  $\delta = 14.12$ , 15.44, 22.69, 28.97, 29.21, 29.28, 29.35, 29.55, 29.62, 29.64, 29.67, 29.73, 29.74, 31.80, 31.92, 32.16, 40.80, 42.26, 109.88, 117.54, 120.28, 122.06, 124.26, 125.38, 126.51, 130.58, 134.96, 136.67, 136.78, 137.08, 143.08, 148.21, 149.23, 149.27 ppm; ESIMS ( $\text{CH}_2\text{Cl}_2/\text{MeOH}$  9:1):  $m/z$ : 1076.6  $[\text{M}+\text{H}]^+$ ; elemental analysis calcd (%) for  $\text{C}_{67}\text{H}_{90}\text{N}_6\text{O}_2 \cdot 1.53\text{H}_2\text{O}$ : C 72.95, H 8.50, N 7.62; found: C 72.90, H 8.37, N 7.98.

**Preparation of the complexes  $[\text{Ln}_2(\text{L11}-2\text{H})_3]$  (Ln = La, Lu):** Ligand **L11** (20 mg,  $2.98 \times 10^{-5}$  mol, 3 equiv) and  $\text{Ln}(\text{OTf})_3 \cdot x\text{H}_2\text{O}$  ( $2.00 \times 10^{-5}$  mol, 2 equiv) were suspended in  $\text{CH}_3\text{CN}$  (50 mL) and sonicated until complete dissolution of **L11** (30 min).  $n\text{Bu}_4\text{NOH} \cdot 30\text{H}_2\text{O}$  (47.68 mg,  $5.96 \times 10^{-5}$  mol, 6 equiv) in  $\text{CH}_3\text{CN}$  (20 mL) were added. The resulting mixture was stirred at RT for one hour. The solution was then evaporated to dryness and the crude product dried under vacuum at 50 °C for 24 h. The red powder was solubilized in  $[\text{D}_6]\text{DMSO}$  for  $^1\text{H NMR}$  analysis.

**Preparation of the complexes  $[\text{Ln}_2\text{Ag}_2(\text{L12}^{\text{C3}}-2\text{H})_3][\text{OTf}]_2$  (Ln=La, Eu, Lu):** Ligand **L12<sup>C3</sup>** (20 mg,  $2.43 \times 10^{-5}$  mol, 3 equiv) was dissolved in  $\text{CH}_2\text{Cl}_2/\text{CH}_3\text{CN}$  (25 mL:25 mL).  $\text{Ln}(\text{OTf})_3 \cdot x\text{H}_2\text{O}$  ( $1.63 \times 10^{-5}$  mol, 2 equiv) and  $n\text{Bu}_4\text{NOH} \cdot 30\text{H}_2\text{O}$  (38.9 mg,  $4.86 \times 10^{-5}$  mol, 6 equiv) were added and a red precipitate rapidly formed. The suspension was stirred at RT for one hour, evaporated to dryness and dried under vacuum. The red insoluble precipitate was suspended in MeOH and sonicated in order to completely solubilize  $n\text{Bu}_4\text{OTf}$ . The red precipitate was filtered, washed with MeOH and dried under vacuum. Elemental analysis of these insoluble amorphous precipitates revealed stoichiometries compatible with  $[\text{Ln}_2(\text{L12}^{\text{C3}}-2\text{H})_3]$  (Ln=La, Eu, Lu) formulae (Table S1 in the Supporting Information). The precipitate was suspended in  $\text{CH}_2\text{Cl}_2/\text{MeOH}$  (25 mL:25 mL) and  $\text{AgOTf}$  (4.2 mg,  $1.63 \times 10^{-5}$  mol, 2 equiv) was added. After 24 h stirring at RT, the precipitate was completely dissolved and the limp orange solution was evaporated to dryness. The orange-red solid was dissolved in methanol, and then crystallized by slow diffusion of diethyl ether. Crystals were filtered and dried under vacuum to yield  $[\text{La}_2\text{Ag}_2(\text{L12}^{\text{C3}}-2\text{H})_3][\text{OTf}]_2 \cdot x\text{H}_2\text{O}$  (Ln=La, Eu, Lu) complexes as red crystals (80%, Table S1 in the Supporting Information). Suitable X-ray quality crystals of  $[\text{La}_2\text{Ag}_2(\text{L12}^{\text{C3}}-2\text{H})_3][\text{OTf}]_2 \cdot 0.5\text{C}_4\text{H}_{10}\text{O} \cdot 0.5\text{CH}_3\text{OH}$  were obtained by using this method, but without final drying.

**Preparation of the complexes  $[\text{Ln}_2(\text{L12}^{\text{C12}}-2\text{H})_3]$  (Ln=La, Lu):** Ligand **L12<sup>C12</sup>** (26.14 mg,  $2.43 \times 10^{-5}$  mol, 3 equiv) was dissolved in  $\text{CH}_2\text{Cl}_2/\text{CH}_3\text{CN}$  (25 mL:25 mL).  $\text{Ln}(\text{OTf})_3 \cdot x\text{H}_2\text{O}$  ( $1.63 \times 10^{-5}$  mol, 2 equiv) and  $n\text{Bu}_4\text{NOH} \cdot 30\text{H}_2\text{O}$  (38.9 mg,  $4.86 \times 10^{-5}$  mol, 6 equiv) were added into this colorless solution. The resulting deep red solution was stirred at RT for 1 hour, evaporated to dryness and dried under vacuum to give a red waxy solid. The crude solid was solubilized in  $\text{CD}_2\text{Cl}_2$  for  $^1\text{H}$  NMR analysis.

**Preparation of the complexes  $[\text{Ln}_2\text{Ag}_2(\text{L12}^{\text{C12}}-2\text{H})_3][\text{OTf}]_2$  (Ln=La, Lu):** Ligand **L12<sup>C12</sup>** (26.14 mg,  $2.43 \times 10^{-5}$  mol, 3 equiv) was dissolved in  $\text{CH}_2\text{Cl}_2/\text{MeOH}$  (25 mL:25 mL). To this colorless solution,  $\text{Ln}(\text{OTf})_3 \cdot x\text{H}_2\text{O}$  ( $1.63 \times 10^{-5}$  mol, 2 equiv),  $\text{AgOTf}$  (4.2 mg,  $1.63 \times 10^{-5}$  mol, 2 equiv) and  $n\text{Bu}_4\text{NOH} \cdot 30\text{H}_2\text{O}$  (38.9 mg,  $4.86 \times 10^{-5}$  mol, 6 equiv) were added. The orange-red solution was stirred at RT for 1 hour, evaporated to dryness and dried under vacuum yielding an orange-red waxy precipitate. The crude solid was solubilized in  $\text{CD}_2\text{Cl}_2$  for  $^1\text{H}$  NMR analysis.

**Spectroscopic and analytical measurements:**  $^1\text{H}$  and  $^{13}\text{C}$  NMR spectra were recorded at 298 K on a Bruker Avance 400 MHz spectrometer. Chemical shifts are given in ppm with respect to TMS. The self-diffusion coefficients in solution ( $\text{CD}_2\text{Cl}_2$ , 298 K) were determined by using diffusion-ordered spectroscopy (DOSY-NMR). The pulse sequence used was the Bruker pulse program `ledbpgp2s`,<sup>[29]</sup> which employs stimulated echo, dipolar gradients and longitudinal eddy current delay as the  $z$  filter. The four 2 ms gradient pulses have sine-bell shapes and amplitudes ranging linearly from 2.5 to 50  $\text{G cm}^{-1}$  in 32 steps. The diffusion delay was in the range 60–140 ms depending on the analyte diffusion coefficient, and the number of scans was 32. The processing was done using a line broadening of 5 Hz and the diffusion coefficients were calculated with the Bruker processing package. Pneumatically-assisted electrospray (ESI-MS) mass spectra were recorded from  $10^{-4}\text{M}$  solutions on an Applied Biosystems API 150EX LC/MS System equipped with a Turbo Ionspray source<sup>®</sup>. Elemental analyses were performed by Dr. H. Eder from the Microchemical Laboratory of the University of Geneva.

**X-ray crystallography:** Summary of crystal data, intensity measurements and structure refinements for  $[\text{La}_2\text{Ag}_2(\text{L12}^{\text{C3}}-2\text{H})_3][\text{CF}_3\text{SO}_3]_2 \cdot 0.5\text{C}_4\text{H}_{10}\text{O} \cdot 0.5\text{CH}_3\text{OH}$  are collected in Table S3 in the Supporting Information. The crystal was mounted on a quartz fiber with protection oil. Cell dimensions and intensities were measured at 150 K on a Stoe IPDS diffractometer with graphite-monochromated  $\text{MoK}\alpha$  radiation ( $\lambda = 0.71073 \text{ \AA}$ ). Data were corrected for Lorentz and polarization effects and for absorption. The structure was solved by direct methods (SIR97),<sup>[30]</sup> all other calculation were performed with SHELXL97<sup>[31]</sup> and ORTEP<sup>[32]</sup> programs. CCDC-794654 contains the supplementary crystallographic data for this paper. These data can be obtained free of charge from The Cambridge Crystallographic Data Centre via [www.ccdc.cam.ac.uk/data\\_request/cif](http://www.ccdc.cam.ac.uk/data_request/cif).

**Comments on the crystal structure of  $[\text{La}_2\text{Ag}_2(\text{L12}^{\text{C3}}-2\text{H})_3][\text{CF}_3\text{SO}_3]_2 \cdot 0.5\text{C}_4\text{H}_{10}\text{O} \cdot 0.5\text{CH}_3\text{OH}$ :** All hydrogen atoms were calculated

and fixed. No significant hydrogen bonding or stacking interactions were detected. Two ethyl groups bound to benzimidazole rings (C48B–C49B and C46B–C47B), two terminal alkyls chains (C43B–C45B and C43C–C45C) and one ionic triflate (S2T) were disordered and were refined with Uiso. Two half molecules of solvent ( $\text{Et}_2\text{O}$  and  $\text{CH}_3\text{OH}$ ) were present in the asymmetric unit. They were refined with Uiso and with population parameters of 0.5.

#### Molecular dynamics (MD) methodology

**Force field:** All MD simulations were carried out with the AMBER 9 software<sup>[33]</sup> and the generalized Amber force field (GAFF) parameters.<sup>[34]</sup> Atomic charges on ligands were calculated with the CHelpG method<sup>[35]</sup> by fitting the electrostatic potential derived from HF/6-31G\* calculations. The Lennard–Jones parameters used for  $\text{La}^{\text{III}}$  were  $R_{\text{La}}^* = 2.105 \text{ \AA}$  and  $\epsilon_{\text{La}} = 0.06 \text{ kcal mol}^{-1}$ . These parameters were developed to reproduce the free energy of hydration of this cation.<sup>[36]</sup> The Lennard–Jones parameters for  $\text{Ag}^{\text{I}}$  were  $R_{\text{Ag}}^* = 1.600 \text{ \AA}$  and  $\epsilon_{\text{Ag}} = 0.345 \text{ kcal mol}^{-1}$ , while for  $\text{Tl}^{\text{I}}$   $R_{\text{Tl}}^* = 1.960 \text{ \AA}$  and  $\epsilon_{\text{Tl}} = 0.355 \text{ kcal mol}^{-1}$  were used. The nonbonded cut-off was set to 12.0  $\text{ \AA}$ .

**Gas-phase molecular dynamics simulations.** Using the conjugated gradient algorithm, an energy minimization of 2000 steps was performed. The system was heated up to 300 K during the first 50 ps of the simulation. After a 950 ps simulation to let the system equilibrate, a 19 ns simulation was performed with the SANDER program within the AMBER 9 package.

**Molecular dynamics simulations in solution ( $\text{CH}_2\text{Cl}_2$ ):** The complexes were solvated by a truncated octahedron box of dichloromethane molecules. The long-range electrostatic interactions were treated with the particle-mesh Ewald method (PME)<sup>[37]</sup> and periodic boundary conditions were applied. The ff03 modified version<sup>[38]</sup> of the parm99 force field was used for the solvent molecules. The SHAKE algorithm was used to constraint bonds involving hydrogen atoms.<sup>[39]</sup> The PMEMD program was used for the MD in solution. Like in the gas phase dynamics, an initial energy minimization of 2000 steps using the conjugated gradient algorithm was performed. During the initial 50 ps of the simulation, the system was heated up to 300 K at constant volume (NVE). This was followed by 950 ps simulation at constant pressure (NPT) to equilibrate the system at 300 K and 1.0 atm. Production runs were performed up to 20 ns (except for complex  $[\text{La}_2\text{Ag}_2(\text{L12}^{\text{C12}}-2\text{H})_3]^{2+}$ , 5 ns) of the total simulation duration in the NPT ensemble with a 2 fs time step.

## Acknowledgements

The authors acknowledge the contributions of the Sciences Mass Spectrometry (SMS) platform at the Faculty of Sciences, University of Geneva, for mass spectrometry services. Financial support from the Swiss National Science Foundation is gratefully acknowledged.

- [1] a) E. C. Constable, *Tetrahedron* **1992**, *48*, 10013–10059; b) E. C. Constable, *Prog. Inorg. Chem.* **1994**, *42*, 67–138; c) C. Piguet, G. Bernardinelli, G. Hopfgartner, *Chem. Rev.* **1997**, *97*, 2005–2062; d) M. Albrecht, *Chem. Rev.* **2001**, *101*, 3457–3497; e) J. Hamacek, *J. Alloys Compd.* **2008**, *451*, 347–351; f) C. Piguet, J.-C. G. Bünzli in *Handbook on the Physics and Chemistry of Rare Earths, Vol. 40* (Eds.: K. A. Gschneidner, Jr., J.-C. G. Bünzli, V. K. Pecharsky), Elsevier, Amsterdam, **2009**, pp. 301–553.
- [2] Y. Morita, Y. Yakiyama, S. Nakazawa, T. Murata, T. Ise, D. Hashizume, D. Shiomi, K. Sato, M. Kitagawa, K. Nakasuji, T. Takui, *J. Am. Chem. Soc.* **2010**, *132*, 6944–6946, and references therein.
- [3] N. Ouali, J.-P. Rivera, P.-Y. Morgantini, J. Weber, C. Piguet, *Dalton Trans.* **2003**, 1251–1263.
- [4] a) H. Wang, S. Ashhab, F. Nori, *Phys. Rev. A* **2009**, *79*, 042335; b) M. Mehring, W. Scherer, A. Weidinger, *Phys. Rev. Lett.* **2004**, *93*, 206603.
- [5] a) J.-C. G. Bünzli, A.-S. Chauvin, C. D. B. Vandevyver, S. Bo, S. Comby, *Ann. N. Y. Acad. Sci.* **2008**, *1130*, 97–105; b) C. M. G. dos

- Santos, A. J. Harte, S. J. Quinn, T. Gunnlaugsson, *Coord. Chem. Rev.* **2008**, *252*, 2512–2527; c) J.-C. G. Bünzli, *Chem. Lett.* **2009**, *38*, 104–109; d) J.-C. G. Bünzli, *Chem. Rev.* **2010**, *110*, 2729–2755.
- [6] a) M. Cantuel, G. Bernardinelli, D. Imbert, J.-C. G. Bünzli, G. Hopfgartner, C. Piguet, *Dalton Trans.* **2002**, 1929–1940; b) D. Imbert, M. Cantuel, J.-C. G. Bünzli, G. Bernardinelli, C. Piguet, *J. Am. Chem. Soc.* **2003**, *125*, 15698–15699; c) S. Torelli, D. Imbert, M. Cantuel, G. Bernardinelli, S. Delahaye, A. Hauser, J.-C. G. Bünzli, C. Piguet, *Chem. Eur. J.* **2005**, *11*, 3228–3242.
- [7] a) C. Piguet, J.-C. G. Bünzli, G. Bernardinelli, G. Hopfgartner, A. F. Williams, *J. Am. Chem. Soc.* **1993**, *115*, 8197–8206; b) N. Martin, J.-C. G. Bünzli, V. McKee, C. Piguet, G. Hopfgartner, *Inorg. Chem.* **1998**, *37*, 577–589; c) S. Floquet, N. Ouali, B. Bocquet, G. Bernardinelli, D. Imbert, J.-C. G. Bünzli, G. Hopfgartner, C. Piguet, *Chem. Eur. J.* **2003**, *9*, 1860–1875; d) K. Zeckert, J. Hamacek, J.-M. Senegas, N. Dalla-Favera, S. Floquet, G. Bernardinelli, C. Piguet, *Angew. Chem.* **2005**, *117*, 8168–8172; *Angew. Chem. Int. Ed.* **2005**, *44*, 7954–7958.
- [8] a) K. Kuriki, Y. Koike, Y. Okamoto, *Chem. Rev.* **2002**, *102*, 2347–2356; b) S. Petoud, *Chimia* **2009**, *63*, 745–752 and references therein; c) A. Mech, A. Monguzzi, F. Meinardi, J. Mezyk, G. Macchi, R. Tubino, *J. Am. Chem. Soc.* **2010**, *132*, 4574–4576.
- [9] a) S. Comby, J.-C. G. Bünzli in *Handbook on the Physics and Chemistry of Rare Earths, Vol. 37* (Eds.: K. A. Gschneidner, Jr., J.-C. G. Bünzli, V. K. Pecharsky), Elsevier, Amsterdam, **2007**, pp. 217–470; b) A. Dossing, *Eur. J. Inorg. Chem.* **2005**, 1424–1434.
- [10] a) K. Binnemans, C. Görrler-Walrand, *Chem. Rev.* **2002**, *102*, 2303–2346; b) K. Binnemans, *Chem. Rev.* **2005**, *105*, 4148–4204; c) C. Piguet, J.-C. G. Bünzli, B. Donnio, D. Guillon, *Chem. Commun.* **2006**, 3755–3768; d) B. Donnio, S. Buathong, I. Bury, D. Guillon, *Chem. Soc. Rev.* **2007**, *36*, 1495–1513; e) K. Binnemans, *J. Mater. Chem.* **2009**, *19*, 448–453.
- [11] M. Albrecht, O. Ossetska, J. Klankermayer, R. Fröhlich, F. Gumy, J.-C. G. Bünzli, *Chem. Commun.* **2007**, 1834–1836.
- [12] a) N. M. Shavaleev, R. Scopelliti, F. Gumy, J.-C. G. Bünzli, *Inorg. Chem.* **2008**, *47*, 9055–9068; b) N. M. Shavaleev, R. Scopelliti, F. Gumy, J.-C. G. Bünzli, *Inorg. Chem.* **2009**, *48*, 6178–6191.
- [13] a) M. Albrecht, O. Ossetska, R. Fröhlich, J.-C. G. Bünzli, A. Aebischer, F. Gumy, J. Hamacek, *J. Am. Chem. Soc.* **2007**, *129*, 14178–14179; b) M. Albrecht, O. Ossetska, J.-C. G. Bünzli, F. Gumy, R. Fröhlich, *Chem. Eur. J.* **2009**, *15*, 8791–8799.
- [14] K. Hiratani, M. Albrecht, *Chem. Soc. Rev.* **2008**, *37*, 2413–2421, and references therein.
- [15] E. Terazzi, L. Guénée, B. Bocquet, J.-F. Lemonnier, N. Dalla Favera, C. Piguet, *Chem. Eur. J.* **2009**, *15*, 12719–12732.
- [16] M. Albrecht, M. Fiege, O. Ossetska, *Coord. Chem. Rev.* **2008**, *252*, 812–824.
- [17] A. Dondoni, *Angew. Chem.* **2008**, *120*, 9133–9135; *Angew. Chem. Int. Ed.* **2008**, *47*, 8995–8997.
- [18] The minute quantity of protonated multi-stranded helical complexes detected by ESI-MS probably results from protonation of the terminal negatively charged oxygen dipoles in  $[\text{Lu}(\text{Lk}-2\text{H})_2+2\text{H}]^{2+}$  ( $k=9, 11$ ), and oxygen tripods in  $[\text{Ln}(\text{Lk}-2\text{H})_3+2\text{H}]^{2+}$  ( $k=9, 11$ , Ln = La, Lu), as inferred from the structure of  $[\text{KEr}(\text{L4}-\text{H})_3]^+$ , whereby  $\text{K}^+$  is bound to the oxygen tripod.<sup>[11]</sup>
- [19] The  $^1\text{H}$  NMR spectra of  $[\text{Ln}(\text{Lk}-2\text{H})_3]$  ( $k=9, 11$ ) indeed display a myriad of weak broad signals contributing to a wavy baseline, typical for polymeric systems in slow exchange on the NMR time scale.
- [20] a) J.-M. Lehn, *Chem. Eur. J.* **1999**, *5*, 2455–2463; b) M. Albrecht, *J. Inclusion Phenom. Macrocyclic Chem.* **2000**, *36*, 127–151; c) M. Ziegler, J. J. Miranda, U. N. Andersen, D. W. Johnson, J. A. Leary, K. N. Raymond, *Angew. Chem.* **2001**, *113*, 755–758; *Angew. Chem. Int. Ed.* **2001**, *40*, 733–736; d) J.-M. Lehn, A. V. Eliseev, *Science* **2001**, *291*, 2331–2333; e) R. F. Ludlow, S. Otto, *J. Am. Chem. Soc.* **2010**, *132*, 5984–5986.
- [21] R. G. Pearson *Survey of Progress in Chemistry, Vol. 5* (Ed.: A. Scott), Academic Press, New York, **1969**, 1–52.
- [22] a) P. S. Pregosin, E. Martinez-Viviente, P. G. A. Kumar, *Dalton Trans.* **2003**, 4007–4014; b) Y. Cohen, L. Avram, L. Frish, *Angew. Chem.* **2005**, *117*, 524–560; *Angew. Chem. Int. Ed.* **2005**, *44*, 520–554; c) A. Macchioni, G. Ciancaleoni, C. Zuccaccia, D. Zuccaccia, *Chem. Soc. Rev.* **2008**, *37*, 479–489; d) S. Augé, P.-O. Schmit, C. A. Crutchfield, M. T. Islam, D. J. Harris, E. Durand, M. Clemancey, A.-A. Quoineaud, J.-M. Lancelin, Y. Prigent, F. Taulelle, M.-A. Delsuc, *J. Phys. Chem. B* **2009**, *113*, 1914–1918.
- [23] a) I. D. Brown, D. Altermatt, *Acta Crystallogr. Sect. B* **1985**, *41*, 244–247; b) N. E. Breese, M. O’Keeffe, *Acta Crystallogr. Sect. B* **1991**, *47*, 192–197; c) I. D. Brown, *Acta Crystallogr. Sect. B* **1992**, *48*, 553–572; d) I. D. Brown, *The Chemical Bond in Inorganic Chemistry*, Oxford University Press, Oxford, **2002**; e) A. Trzesowska, R. Kruszynski, T. J. Bartczak, *Acta Crystallogr. Sect. B* **2004**, *60*, 174–178; f) A. Trzesowska, R. Kruszynski, T. J. Bartczak, *Acta Crystallogr. Sect. B* **2005**, *61*, 429–434; g) F. Zocchi, *J. Mol. Struct. THEO-CHEM* **2007**, *805*, 73–78; h) I. D. Brown, *Chem. Rev.* **2009**, *109*, 6858–6919.
- [24] This exchange process is so fast that VT- $^1\text{H}$  NMR spectroscopy at the lowest accessible temperature (183 K) in  $\text{CD}_2\text{Cl}_2$  does not affect the global  $D_3$  symmetry of the spectrum (Figure S14 in the Supporting Information).
- [25] a) M. L. Connolly, *Science* **1983**, *221*, 709–713; b) M. L. Connolly, *J. Appl. Crystallogr.* **1983**, *16*, 548–558.
- [26] a) A. El-ghayoury, L. Douce, A. Skoulios, R. Ziessel, *Angew. Chem.* **1998**, *110*, 2327–2331; *Angew. Chem. Int. Ed.* **1998**, *37*, 2205–2208; b) L. Douce, A. El-ghayouri, A. Skoulios, R. Ziessel, *Chem. Commun.* **1999**, 2033–2034; c) R. Ziessel, L. Douce, A. El-ghayoury, A. Harriman, A. Skoulios, *Angew. Chem.* **2000**, *112*, 1549–1553; *Angew. Chem. Int. Ed.* **2000**, *39*, 1489–1493.
- [27] J. F. Desreux in *Lanthanide Probes in Life, Chemical and Earth Sciences* (Eds.: J.-C. G. Bünzli, G. R. Choppin), Elsevier, Amsterdam, **1989**, Chapter 2, p. 43.
- [28] G. Schwarzenbach, *Complexometric Titrations*, Chapman & Hall, London, **1957**, p. 8.
- [29] D. Wu, A. Chen, C. S. Johnson, Jr., *J. Magn. Reson. Ser. A* **1995**, *115*, 260–264.
- [30] A. Altomare, M. C. Burla, M. Camalli, G. Cascarano, C. Giacovazzo, A. Guagliardi, G. Moliterni, G. Polidori, R. Spagna, *J. Appl. Crystallogr.* **1999**, *32*, 115–119.
- [31] SHELXL97, Program for the Solution and Refinement of Crystal Structures, G. M. Sheldrick, University of Göttingen (Germany), **1997**.
- [32] ORTEP II, Report ORNL-5138, C. K. Johnson, Oak Ridge National Laboratory, Oak Ridge, **1976**.
- [33] AMBER 9, D. A. Case, T. A. Darden, I. Cheatham, C. L. Simmerling, J. Wang, R. E. Duke, R. Luo, K. M. Merz, D. A. Pearlman, M. Crowley, R. C. Walker, W. Zhang, B. Wang, S. Hayik, A. Roitberg, G. Seabra, K. F. Wong, F. Paesani, X. Wu, S. Brozell, V. Tsui, H. Gohlke, L. Yang, C. Tan, J. Mongan, V. Hornak, G. Cui, P. Beroza, D. H. Mathews, C. Schafmeister, W. S. Ross, P. A. Kollman, **2006**, University of California, San Francisco.
- [34] J. M. Wang, R. M. Wolf, J. W. Caldwell, P. A. Kollman, D. A. Case, *J. Comput. Chem.* **2004**, *25*, 1157–1174.
- [35] C. M. Breneman, K. B. Wiberg, *J. Comput. Chem.* **1990**, *11*, 361–373.
- [36] F. C. J. M. van Veggel, D. N. Reinhoudt, *Chem. Eur. J.* **1999**, *5*, 90–95.
- [37] T. Darden, D. York, L. Pedersen, *J. Chem. Phys.* **1993**, *98*, 10089–10092.
- [38] Y. Duan, C. Wu, S. Chowdhury, M. C. Lee, G. M. Xiong, W. Zhang, R. Yang, P. Cieplak, R. Luo, T. Lee, J. Caldwell, J. M. Wang, P. A. Kollman, *J. Comput. Chem.* **2003**, *24*, 1999–2012.
- [39] W. F. Van Gunsteren, H. J. C. Berendsen, *Mol. Phys.* **1977**, *34*, 1311–1327.

Received: September 27, 2010

Published online: December 3, 2010